

PREPARED FOR SUBMISSION TO JHEP

# Jet Flavour Tagging at FCC-ee with a Transformer-based Neural Network: DeepJetTransformer

Freya Blekman <sup>1,2,4</sup> Florencia Canelli <sup>3</sup> Alexandre De Moor <sup>1</sup> Kunal Gautam <sup>1,3</sup> Armin Ilg <sup>3</sup> Anna Macchiolo <sup>3</sup> Eduardo Ploerer <sup>1,3</sup>

<sup>1</sup>*Inter-university Institute for High Energies, Vrije Universiteit Brussel, 1050 Brussels, Belgium*

<sup>2</sup>*Deutsches Elektronen-Synchrotron DESY, Notkestr. 85, 22607 Hamburg, Germany*

<sup>3</sup>*Universität Zürich, Winterthurerstr. 190, 8057 Zürich, Switzerland*

<sup>4</sup>*Universität Hamburg, Luruper Chaussee 149, 22761 Hamburg, Germany*

*E-mail:* [kunal.gautam@cern.ch](mailto:kunal.gautam@cern.ch), [eduardo.ploerer@cern.ch](mailto:eduardo.ploerer@cern.ch)

**ABSTRACT:** Jet flavour tagging is crucial in experimental high-energy physics. A tagging algorithm, **DeepJetTransformer**, is presented, which exploits a transformer-based neural network that is substantially faster to train.

The **DeepJetTransformer** network uses information from particle flow-style objects and secondary vertex reconstruction as is standard for  $b$ - and  $c$ -jet identification supplemented by additional information, such as reconstructed  $V^0$ s and  $K^\pm/\pi^\pm$  discrimination, typically not included in tagging algorithms at the LHC. The model is trained as a multiclassifier to identify all quark flavours separately and performs excellently in identifying  $b$ - and  $c$ -jets. An  $s$ -tagging efficiency of 40% can be achieved with a 10%  $ud$ -jet background efficiency. The impact of including  $V^0$ s and  $K^\pm/\pi^\pm$  discrimination is presented.

The network is applied on exclusive  $Z \rightarrow q\bar{q}$  samples to examine the physics potential and is shown to isolate  $Z \rightarrow s\bar{s}$  events. Assuming all other backgrounds can be efficiently rejected, a  $5\sigma$  discovery significance for  $Z \rightarrow s\bar{s}$  can be achieved with an integrated luminosity of  $60 \text{ nb}^{-1}$ , corresponding to less than a second of the FCC-ee run plan at the  $Z$  resonance.

---

## Contents

<b>1</b>	<b>Introduction</b>	<b>2</b>
<b>2</b>	<b>Experimental Environment</b>	<b>3</b>
2.1	FCC-ee	3
2.2	IDEA Detector Concept	3
2.3	Event Samples and Jet Reconstruction	4
<b>3</b>	<b>Vertex Reconstruction</b>	<b>4</b>
3.1	$V^0$ Vertex Reconstruction	5
3.2	Secondary Vertex Reconstruction	6
<b>4</b>	<b>DeepJetTransformer</b>	<b>7</b>
4.1	Input Features	7
4.2	Transformer Models	9
4.2.1	Scaled Dot-Product Attention and Heavy Flavour Transformer Block	10
4.2.2	DeepJetTransformer Architecture	12
4.2.3	Training Methodology	13
<b>5</b>	<b>Classifier Performance</b>	<b>13</b>
5.1	Qualitative Comparison with Other Taggers	17
5.2	Dependence on the Quality of Particle Identification	19
5.3	Dependence on the Presence of Neutral Kaons	20
5.4	Importance of Variable Classes and Individual Variables	20
5.5	Dependence on the Flavour Definition	22
<b>6</b>	<b>Example of Performance: The <math>Z</math> Boson at the FCC-ee</b>	<b>22</b>
6.1	Physics Potential at the $Z$ Resonance	23
6.2	Event and Jet Selection	24
6.3	Performance and Working Points	24
<b>7</b>	<b>Outlook</b>	<b>27</b>
<b>8</b>	<b>Conclusion</b>	<b>28</b>

---

# 1 Introduction

The Standard Model (SM) of particle physics is one of the most successful scientific theories describing the fundamental particles and their interactions. The last piece of this model, the Higgs boson, was discovered [1, 2] at the Large Hadron Collider (LHC) [3] in 2012, and the precise study of its properties will remain mostly superficial at the LHC due to high irreducible backgrounds from other SM processes while isolating Higgs boson events.

One of the main motivations for proposed future lepton colliders [4–7] is the precise measurement of SM parameters, like precision studies of the hadronic decay of the  $Z$  boson and greatly improved sensitivity to the couplings of the Higgs boson to the bottom ( $b$ ) and charm ( $c$ ) quarks and gluons ( $g$ ) [8–10]. Achieving these objectives requires an efficient reconstruction and identification of the hadronic decays of these particles. The feasibility of studying the decay of the Higgs boson to the strange ( $s$ ) and the light quarks depends on the collider and detector performance and is currently under investigation in the field. It is well established that efficient and accurate jet flavour identification is essential to exploit the maximal physics potential of future collider experiments [11–15].

Jets originating from the  $b$  and  $c$  quarks contain hadrons with significant lifetimes that travel distances of the order of millimeters from the interaction point before decaying into lighter hadrons. The heavy flavour tagging algorithms used at the Large Electron-Positron collider (LEP) [16, 17] and the Tevatron [18, 19] experiments exploited variables derived from the displaced charged tracks originating from these decayed  $B$  (containing  $b$  quark) or  $D$  (containing  $c$  quark) hadrons to distinguish the heavy flavoured jets from the light quark and gluon jets. These charged tracks are commonly clustered to reconstruct the original decay vertices of the  $B$  and  $D$  hadrons, also called secondary vertices (SVs). The properties of these SVs, like their mass and displacement, can also be used to identify  $b$ - and  $c$ -jets.

The understanding and performance of jet flavour tagging at the LHC has steadily been improving and heavily relies on machine learning (ML) [20, 21], which also inspires flavour tagging algorithms for the FCC-ee [22, 23]. The cleaner environment at lepton colliders and the powerful capabilities of the proposed detectors, such as particle identification (PID), improve the performance of heavy flavour tagging and new analysis techniques, including strange jet tagging, become feasible. Strange jets tend to have a higher kaon multiplicity and a lower number of pions than light jets. Therefore distinguishing  $K^\pm$  and  $\pi^\pm$  and reconstructing  $K_S^0$  is crucial for strange jet identification [24–26].

ML approaches are uniquely suited to classify jet flavours, where training samples are abundant in the form of Monte Carlo (MC) simulation. Still, the underlying dynamics of jet formation and hadronisation are not always well understood. With the advent of Neural Networks (NNs) to jet classification, approaches relying on single physics-motivated variables for jet flavour discrimination were significantly outperformed [21]. Since then, a multitude of architectures and jet representations have found success in discriminating jet flavours, including Dense Neural Networks (DNNs) [27], Recurrent Neural Networks (RNNs) [28], Convolutional Neural Networks (CNNs) [29, 30], and Graph Neural Networks (GNNs) [22, 31].

Among the most successful of these are Graph-based architectures such as **ParticleNet** [22] that represent jets as sets of nodes (jet constituents) and edges (some pairwise defined feature, often the difference in a given variable of jet constituents). In particular, networks combining a self-attention mechanism to exploit the relative importance of constructed features, dubbed Transformer Networks, have achieved state-of-the-art performance. Particle Transformer (ParT) [32] combines a graph representation of jets with an attention mechanism. A pure Transformer architecture based on Ref. [33], which is relatively lightweight and requires much less computational time compared to the state-of-the-art, for example ParT, yet achieves comparable tagging performance, is presented in this work for the task of jet flavour identification at future lepton colliders, using the FCC-ee with the IDEA detector concept as a benchmark [4, 34].

Section 2 summarises the FCC-ee collider, the IDEA detector concept, and the used simulated samples and provides minimal event selection requirements. Section 3 briefly describes the algorithms used to reconstruct displaced decay vertices and their performance. Section 4 introduces the attention mechanism and Transformer models and outlines the description of the input features and the network architecture used for tagging. Finally, the obtained results and the performance of the flavour-tagging algorithm in Z boson signatures are presented in Section 5 and 6, respectively.

## 2 Experimental Environment

### 2.1 FCC-ee

The Future Circular Collider (FCC) integrated project [35, 36] aims to build  $e^+e^-$ ,  $pp$ , and  $ep$  colliders in a 90.7 km circular tunnel in the Geneva region. FCC-ee [4] is a proposed  $e^+e^-$  collider and the first stage of the FCC integrated project. It is currently planned to run at four different center-of-mass energy modes, starting from around 91.2 GeV at the Z-pole to 365 GeV, over the  $t\bar{t}$  threshold. The unprecedented luminosities at the FCC-ee uniquely facilitate tests of the SM and, at the same time, present novel challenges in reducing systematic errors. The circular collider design provides the opportunity for multiple interaction points, each of which can host a different detector design. Three such detector concepts [34, 37, 38] are currently being studied, of which the IDEA detector concept [34] has been used in this study.

### 2.2 IDEA Detector Concept

A fast simulation of the IDEA detector concept [39] has been implemented in **Delphes** [40] and used for the simulation of the samples used in this work. The innermost part of the IDEA detector is the monolithic active pixel sensor (MAPS) based vertex detector, which consists of three inner layers with a space point resolution of 3  $\mu\text{m}$ , and two outer barrel and three disk layers on each side with a space point resolution of 7  $\mu\text{m}$ . The innermost layer is currently positioned at a radius of 1.2 cm, however, the event samples were generated assuming the innermost layer at 1.7 cm. The vertex detector is enclosed by the drift

chamber incorporating 112 layers of 100  $\mu\text{m}$  resolution. The multiple scattering of particles is minimal thanks to the main gas component being Helium. Two layers of silicon sensors surround the drift chamber to provide a very precise space point measurement. A single-hit resolution of 7  $\mu\text{m}$  (90  $\mu\text{m}$ ) along  $\phi$  ( $z$ ) is assumed. These sit inside a solenoid magnet with a 2 T magnetic field. It is followed by a dual-readout calorimeter that is sensitive to independent signals from the scintillation and the Cerenkov light production. This results in a good energy resolution for both electromagnetic and hadronic showers. The calorimeter is enveloped by the muon system consisting of layers of chambers embedded in the magnet return yoke.

### 2.3 Event Samples and Jet Reconstruction

The simulated event samples consist of the process  $e^+e^- \rightarrow Z \rightarrow q\bar{q}$ , where  $q \equiv b, c, (u, d, s)$ , at the center-of-mass energy ( $\sqrt{s}$ ) of 91.2 GeV. `Pythia8.303` [41] is used for event generation, parton showering, and hadronisation. `Delphes` [40] is used for event reconstruction assuming the IDEA detector concept [34, 39].

Jet clustering is performed with `FastJet-3.3.4` [42] using the exclusive  $e^+e^- k_T$  algorithm [43]. Other jet clustering algorithms like the anti- $k_T$  algorithm [44] and the generalised  $e^+e^- k_T$ , also referred to as the inclusive  $e^+e^- k_T$ , algorithm [42] were also considered. The exclusive (Durham)  $e^+e^- k_T$  algorithm clustered jets were observed to satisfy the requirements of this study and signature the best.

## 3 Vertex Reconstruction

Vertex reconstruction is essential to find the primary interaction vertex and the secondary decay vertices of the long-lived  $B$ ,  $D$ , and  $S$  (containing  $s$  quark) hadrons. It helps improve the  $b$ - and  $c$ -tagging performance and aids in  $s$ -tagging. Charged tracks can be fitted to reconstruct the primary and the displaced secondary vertices. These displaced vertices can either be the decay vertices of  $B$  and  $D$  hadrons (SVs) or those of the long-lived  $S$  hadrons, like  $K_S^0$  or  $\Lambda^0$ , also known as  $V^0$ s, which are particles that decay into a pair of oppositely charged tracks. The properties of these SVs, such as their masses, displacements, and charged track multiplicities, can be used to identify the decaying hadrons and, in effect, the jet flavour. The SVs can even be used to reconstruct the entire hadronic decay chain. Similarly, reconstructing and identifying the  $V^0$  vertices can be used to identify  $s$ -jets, as  $K_S^0$  and  $\Lambda^0$  are the leading particles in some  $s$ -jets. Distinguishing  $V^0$ s from SVs also helps to reduce the misidentification of some  $b$ - and  $c$ -jets as  $s$ -jets. The vertex reconstruction in this study has been performed using an implementation of the vertexing module of the `LCFIPlus` framework [45, 46] as implemented in `FCCAnalyses` [47], the FCC software framework, using a  $\chi^2$ -based vertex fitter [48].

The properties of these SVs and  $V^0$ s, along with more variables, are used as input to train the neural network tagger described in Section 4.

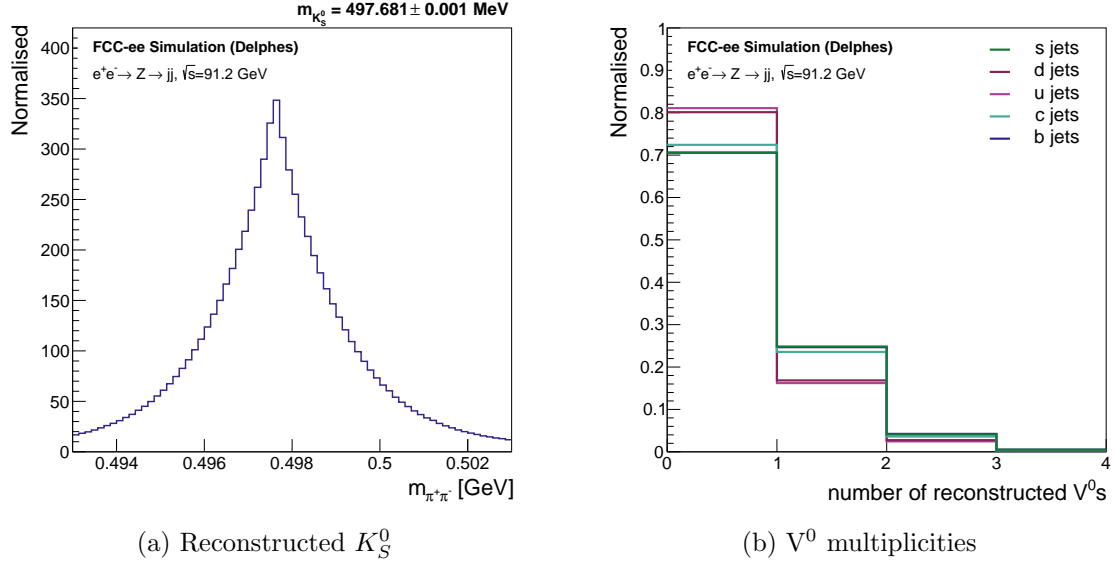


**Figure 1:** Performance of  $V^0$  reconstruction. (a) Invariant mass distribution of reconstructed  $K_S^0$  vertices and (b) reconstructed  $V^0$  multiplicity in jets from  $e^+e^- \rightarrow Z \rightarrow q\bar{q}$  events at  $\sqrt{s} = 91.2$  GeV, where  $q \equiv u, d, s, c, b$ . The quoted mass is the mean and the error on the mean of the distribution.

### 3.1 $V^0$ Vertex Reconstruction

The vertex finding algorithm employed in this study first identifies the tracks forming  $V^0$ s. The tracks originating from the primary vertex or  $V^0$  candidates are not considered while reconstructing SVs.

The  $V^0$ s are found by reconstructing all possible vertices with pairs of oppositely charged tracks and constraining their invariant masses, displacements, and directions. The vertices are not discarded but stored and assigned a particle ID based on the set of constraints that they pass, summarised in Table 1. Three processes are considered:  $K_S^0 \rightarrow \pi^+\pi^-$ ,  $\Lambda^0 \rightarrow p\pi^-$ , and photon conversions,  $\gamma_{conv} X \rightarrow e^+e^-X$ . The Delphes

	$K_S^0$		$\Lambda^0$		$\gamma_{conv}$	
	tight	loose	tight	loose	tight	loose
M [GeV]	[0.493, 0.503]	[0.488, 0.508]	[1.111, 1.121]	[1.106, 1.126]	< 0.005	< 0.01
r [mm]	> 0.5	> 0.3	> 0.5	> 0.3	> 9	> 9
$\hat{p} \cdot \hat{r}$	> 0.999	> 0.999	> 0.99995	> 0.999	> 0.99995	> 0.999

**Table 1:** Summary of the default  $V^0$  selection criteria [45]. M is the invariant mass, and p is the momentum of the  $V^0$  candidate. r is the distance of the  $V^0$  candidate from the primary vertex.  $\hat{p} \cdot \hat{r}$  is defined as a collinearity variable for the  $V^0$  candidate. The set of ‘tight’ constraints has been used to identify  $V^0$ s in this study, while the set of ‘loose’ constraints has been used to reconstruct the seed vertex.

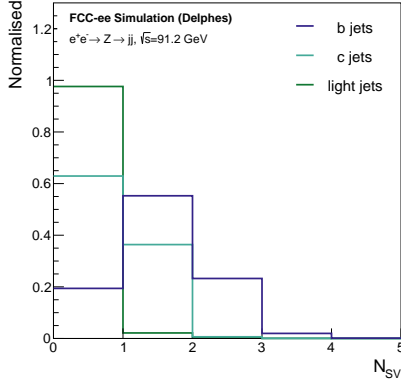
samples used in this study do not simulate photon conversions, therefore the reconstructed  $V^0$ s only contain  $K_S^0$ s and  $\Lambda^0$ s. The invariant mass of the reconstructed  $K_S^0$ s can be seen in Figure 1a. The mass of the decay particles used to calculate the invariant mass of the  $V^0$  is decided based on which set of constraints the  $V^0$  passes, unlike the SV, where all tracks are assumed to be pions in the invariant mass calculation.

Figure 1b displays the  $V^0$  multiplicity in jets from  $Z \rightarrow q\bar{q}$  events. No reconstructed  $V^0$ s are found for most of the jets for every flavour except for strange. The high number of heavy-flavoured jets with one or more reconstructed  $V^0$ s justifies the importance of  $V^0$  rejection before attempting to reconstruct SVs. It is also evident that more  $s$ -jets have one or more reconstructed  $V^0$ s than  $u$ - and  $d$ -jets, making  $V^0$ s an important discriminator  $s$ -jets against light jets.

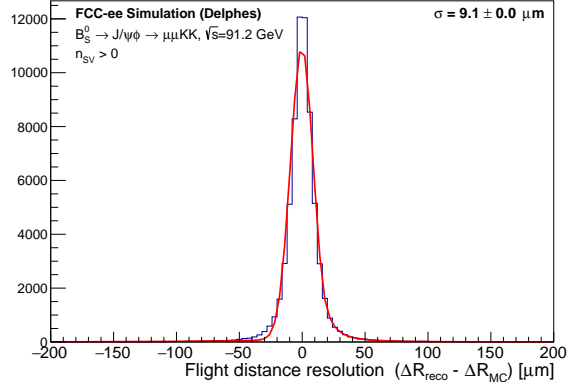
### 3.2 Secondary Vertex Reconstruction

Secondary Vertices are found by reconstructing a two-track vertex (seed) with the lowest  $\chi^2$  from the vertex fit and attaching tracks to this seed, resulting in a vertex with the lowest  $\chi^2$  until the resulting vertex no longer passes the criteria mentioned in Ref. [45]. The tracks forming the SV are stored and removed from the original set, and more SVs are reconstructed recursively until no more seeds pass the required constraint thresholds.

Due to the near-diagonal CKM matrix, the cascading decay chain of heavier quarks is expected to be  $b \rightarrow c \rightarrow s \rightarrow (u, d)$ . Hence, the SV multiplicity tends to be higher in  $b$ -jets compared to  $c$ - and light jets, as can be seen in Figure 2a. The resolution of the flight distance of the SV achieved using this reconstruction in  $B_S^0$  decays can be seen in Figure 2b. The flight distance resolution is defined as the difference between the radial distance of the reconstructed SV from the primary vertex and the radial distance of the MC decay vertex. The closest SV is associated with the MC decay vertex for events with multiple reconstructed SVs.



(a) SV multiplicity in jets from  $e^+e^- \rightarrow Z \rightarrow q\bar{q}$  events



(b) Flight distance resolution in  $10^4 B_S^0 \rightarrow J/\psi\phi \rightarrow \mu\mu KK$  events.

**Figure 2:** Performance of secondary vertex reconstruction in processes generated at  $\sqrt{s} = 91.2$  GeV.

## 4 DeepJetTransformer

Since the introduction of **ParticleNet**, the concept of Particle Cloud has become the prevailing representation of jet structure. A Particle Cloud considers the jet as an unordered set of jet constituents of varying length. Elements of differing nature, such as charged, neutral particles, or SVs associated with the jet, are considered to create the most complete and accurate representation. This representation concept was used to build the presented model, the key element of which, the unordered set of particles, requires the construction of a model invariant under the permutation of the jet constituents. This essential property is in opposition to most Transformer models established around the principle of causality [33, 49]. It was also expected to design a model capable of extracting connections between the jet constituents, enhancing its capabilities of constructing engineered high-level features by capturing dependencies inside the global structure of the jet.

A structure based on Transformer blocks was thus chosen for this study. Previous research has indicated that Transformer models offer enhanced performance and increased efficiency, particularly compared to Graph models [32]. The subsequent sections will elaborate on the inputs to the neural network and the fundamental characteristics of Transformer models and provide a detailed description of the specific model, **DeepJetTransformer**, which has been developed for this study.

### 4.1 Input Features

The properties of each jet and its constituents represent different categories of input features available for model training. The jet kinematics are represented by variables defined using its 4-momentum, as detailed in Table 2. Many future collider detector concepts are designed to be used with a particle flow algorithm [50, 51]. Therefore, jet constituents are subdivided into five sets according to the typical particle flow candidate categories: charged hadrons, neutral hadrons, electrons and positrons ( $e^\pm$ ), photons ( $\gamma$ ), and muons ( $\mu^\pm$ ). Kinematic variables are defined for each jet constituent using its 4-momentum, as listed in Table 3. For each jet up to 25 charged jet constituents and 25 neutral jet constituents are considered. This is enforced by truncating the input feature array of a given jet if the number of charged/neutral jet constituents is more than 25. Conversely, if the number of charged/neutral jet constituents is less than 25, then the input feature array is zero-padded.

Charged tracks are first fitted to find the  $V^0$ s and the remaining tracks are used to reconstruct SVs. Feature variables are defined separately for both classes of reconstructed vertices ( $V^0$ s and SVs) and are listed in Table 4. Up to 4  $V^0$ s and 4 SVs are considered per jet. The  $V^0$  and SV input feature arrays are likewise truncated/zero-padded. The distinguishing power of some of these variables is discussed below.

The jet momentum distribution of  $b$ -jets tends to be more spread out than that of light jets, as seen in Figure 3a. This is due to the longer decay chain in  $b$ -jets, where more momentum can be lost through neutrinos than in light jets.

An important distinguishing variable for  $b$ -jet identification is the transverse impact parameter ( $D_0$ ), which is higher for heavier flavour jets as the decaying  $B$  hadrons have a



Input Feature	Description
$ p , E, m$	momentum, energy, and invariant mass of the jet
$\theta, \phi$	polar and azimuthal angle of the jet axis
$N_{\text{charged}}$	charged particle (track) multiplicity in the jet
$N_{\text{neutral}}$	neutral particle multiplicity in the jet
$\lambda_{\beta}^{\kappa} = \sum_{i \in \text{jet}} z_i^{\kappa} \Theta_i^{\beta}$	jet angularity [52] as sum of normalized jet constituent energy ( $z_i$ ) and angular distance to jet axis ( $\Theta_i$ ) for ( $\kappa = 0, \beta = 0$ ), ( $\kappa = 1, \beta = 0.5$ ), ( $\kappa = 1, \beta = 1$ ), ( $\kappa = 1, \beta = 2$ ), ( $\kappa = 0, \beta = 2$ )
<b>isU/D/S/C/B</b>	MC flavour assigned to the jet

**Table 2:** Description of global features associated with each jet

Input Feature	Description
$D_0(z_0)$	signed transverse (longitudinal) impact parameter
$D_0/\sigma_{D_0}(z_0/\sigma_{z_0})$	signed transverse (longitudinal) impact parameter significance
$\theta_{\text{rel}}(\phi_{\text{rel}})$	polar (azimuthal) angle of track with respect to the jet axis
$\Theta$	angular distance of track and jet axis
$C$	half-curvature of the track
$m_{\text{ch.}}, q$	track invariant mass and charge
$\frac{ p _{\text{ch.}}}{ p _{\text{jet}}}, \ln( p _{\text{ch.}}), \ln\left(\frac{ p _{\text{ch.}}}{ p _{\text{jet}}}\right)$	(normalised) magnitude of track momentum and logarithms
$\frac{E_{\text{ch.}}}{E_{\text{jet}}}, \ln(E_{\text{ch.}}), \ln\left(\frac{E_{\text{ch.}}}{E_{\text{jet}}}\right)$	(normalised) track energy and logarithms
<b>isKaon</b>	if the particle is identified as a $K^{\pm}$
<b>isMuon</b>	if the particle is identified as a $\mu^{\pm}$
<b>isElectron</b>	if the particle is identified as an $e^{\pm}$
$\theta_{\text{rel}}(\phi_{\text{rel}})$	polar (azimuthal) angle of particle with respect to the jet axis
$\Theta$	angular distance of neutral particle and jet axis
$\frac{ p _{\text{neut.}}}{ p _{\text{jet}}}, \ln( p _{\text{neut.}}), \ln\left(\frac{ p _{\text{neut.}}}{ p _{\text{jet}}}\right)$	(normalised) magnitude of particle momentum and logarithms
$\frac{E_{\text{neut.}}}{E_{\text{jet}}}, \ln(E_{\text{neut.}}), \ln\left(\frac{E_{\text{neut.}}}{E_{\text{jet}}}\right)$	(normalised) neutral particle energy and logarithms
<b>isPhoton</b>	if the particle is identified as a Photon

**Table 3:** Description of features associated with each jet constituent. The sets of variables are divided into charged particles (tracks) and neutral particles.

significantly longer lifetime than  $D$  or light hadrons (except for  $V^0$ s). The differentiating effect between flavours caused by this can be seen more clearly in the transverse impact parameter significance, defined as  $S(D_0) = D_0/\sigma_{D_0}$ , where  $\sigma_{D_0}$  is the uncertainty in the measurement of the transverse impact parameter. It is depicted in Figure 3b.

As mentioned in Section 3.2,  $b$ -jets tend to have a higher SV multiplicity than  $c$ - and light jets. It is a dominant property in identifying  $b$ -jets and, to some extent,  $c$ -jets.

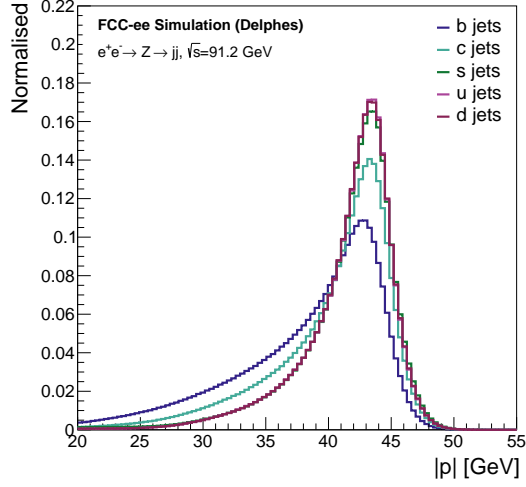
Input Feature	Description
$p, m$	momentum and invariant mass of the SV
$N_{\text{tracks}}$	track multiplicity of the SV
$\chi^2, N_{\text{DoF}}$	$\chi^2$ and number of degrees of freedom of the SV
$\theta_{\text{rel}}, \phi_{\text{rel}}$	polar and azimuthal angle of the SV with respect to the jet axis
$\hat{\mathbf{p}} \cdot \hat{\mathbf{r}}$	collinearity of SV with respect to PV
$d_{3D}, d_{xy}$	3D and transverse distance of the SV from the PV

**Table 4:** Description of features associated with each reconstructed secondary vertex. Similar features, with the addition of PDG ID [53], are also defined for  $V^0$ s while comparing the performance of the tagger trained with and without  $V^0$ s.

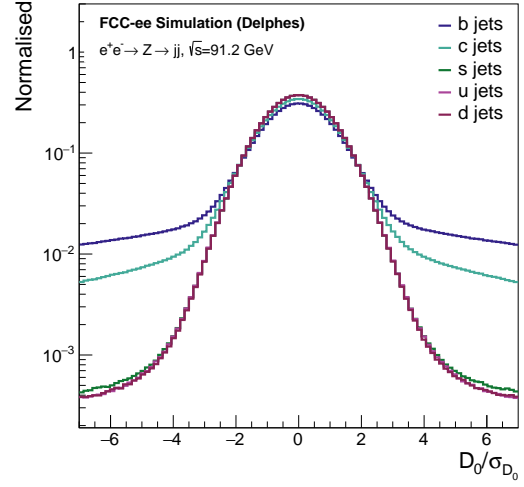
The most challenging background for  $s$ -tagging is  $ud$ -jets. Two powerful distinguishing variables tend to be the multiplicities of charged and neutral Kaons and Pions, exploiting the conservation of strangeness during hadronisation in strange jets. These can be seen in Figure 3c and 3d. To distinguish between  $K^\pm$  and  $\pi^\pm$ , PID techniques like energy loss ( $dE/dx$ ) [54], ionisation cluster counting ( $dN/dx$ ) [55], time-of-flight [56], etc. are traditionally used. The  $K^\pm/\pi^\pm$  classification is generically emulated, instead of relying on any particular PID technique, with a varying efficiency of correctly identifying  $K^\pm$ , the baseline scenario being 90% efficiency, and a 10% efficiency of misidentifying  $\pi^\pm$  as  $K^\pm$ . The baseline PID scenario was deliberately conservative with respect to the state-of-the-art  $K^\pm$  identification and follows PID studies at Belle, which found the average efficiency and fake rate for charged particles between 0.5 and 4 GeV/ $c$  to be  $(87.99 \pm 0.12)\%$  and  $(8.53 \pm 0.10)\%$ , respectively [57]. To further improve PID, neutral strange hadrons ( $K_S^0$  and  $\Lambda^0$ ) are reconstructed in the form of  $V^0$ s, as was shown in Figure 1. These variables, as described in Table 2, 3, and 4, are fed into a neural network, the architecture of which is described below.

## 4.2 Transformer Models

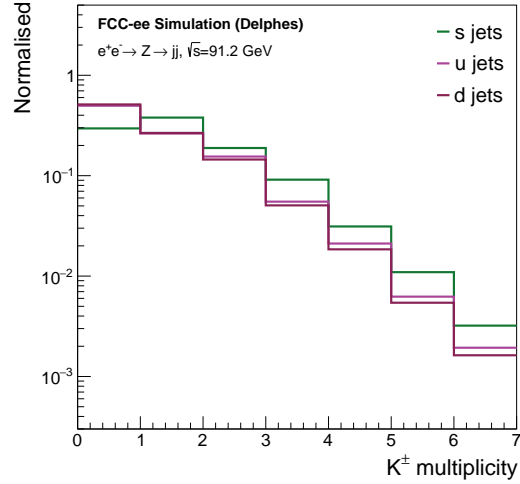
Inspired by the success of attention mechanism in Natural Language Processing (NLP) [33, 49] or Computer Vision (CV) [58] tasks, this model adopts Transformer blocks as its primary architectural component. Transformers belong to a class of neural networks that leverage the scaled dot-product attention mechanism [33]. The attention mechanism enables the model to selectively focus on specific segments of the input sequence while processing each constituent element. In contrast to earlier architectures, such as recurrent models that utilise fixed-size windows or recurrent connections, the attention mechanism dynamically assigns weights to individual elements within the jet based on their relevance, capturing intricate dependencies across the entirety of the jet structure. This adaptive and global weighting scheme empowers the Transformer to effectively model contextual information, a crucial element for understanding and generating coherent high-level features.



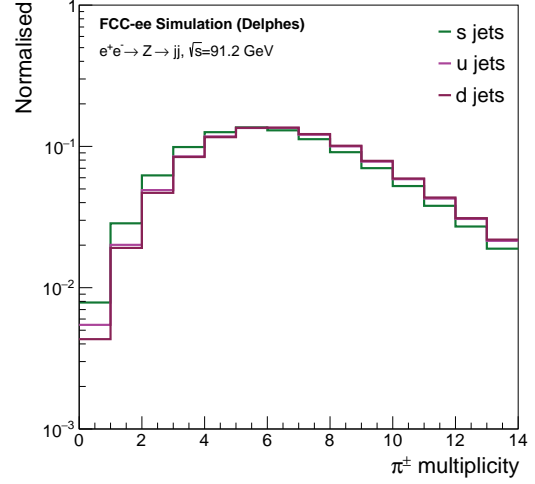
(a) Jet Momentum.



(b) Transverse impact parameter significance.



(c) Kaon multiplicities.



(d) Pion multiplicities.

**Figure 3:** Distinguishing features in the clustered jets of  $e^+e^- \rightarrow Z \rightarrow q\bar{q}$  events at  $\sqrt{s} = 91.2$  GeV, separated by flavour. Fig 3b corresponds to the jet constituents, the rest correspond to the clustered jets. The IDEA detector concept was used for reconstruction.

#### 4.2.1 Scaled Dot-Product Attention and Heavy Flavour Transformer Block

The scaled dot-product attention (SDPA) mechanism uses three inputs: a query matrix  $Q$ , a key matrix  $K$ , and a value matrix  $V$ . The query matrix represents the items for which the attention weights are computed, while the key and value matrices represent all items in the sequence. After being fed into linear layers, the query tensor  $Q$  of dimension  $(B, N, d_k)$ , the key tensor  $K$  of dimension  $(B, L, d_k)$ , and the value tensor  $V$  of dimension

$(B, L, d'_k)$  are fed into the scaled dot-product attention as:

$$\text{Attention}(Q, K, V) = \text{SoftMax}\left(\frac{QK^T}{\sqrt{d_k}}\right)V. \quad (4.1)$$

The attention mechanism in this study is employed in a specific configuration where the query, key, and value tensors are identical. This particular case is commonly referred to as self-attention. The output tensors  $Q$ ,  $K$ , and  $V$  are generated through linear layers, facilitating the transformation and projection of the input tensors to the attention space.

SDPA is extended to enhance the discriminating power of the model by allowing it to attend to multiple subspaces of attention in parallel. This extension, referred to as Multi-Head Attention (MHA), facilitates the capture of diverse and complementary high-level features from the input by projecting the Query, Key, and Value matrices independently for each of the  $h$  attention heads. Each attention head performs an SDPA operation, yielding distinct representations. These head representations are then concatenated and passed through a linear layer to integrate the information across heads. The MHA layer can mathematically be represented by the following equations:

$$\text{MHA}(Q, K, V) = \text{Concat}(h_1, \dots, h_n)W^O, \quad (4.2)$$

$$h_i = \text{Attention}(QW^{Q,i}, KW^{K,i}, VW^{V,i}). \quad (4.3)$$

The presented approach, employing the Particle Cloud representation, intentionally refrains from employing positional encoding. This decision stems from the absence of a hierarchical structure or positional ordering among the components of the jets, in contrast to sequences such as sentences or image patches. Consequently, the MHA module operates without incorporating positional encoding and instead only leverages permutation invariant mechanisms to capture and process the interrelationships between particles in the jet, yielding meaningful results. The permutation invariance of **DeepJetTransformer** is established by the properties of permutation equivariance and invariance of function composition. The permutation equivariance of each function of the transformer blocks ensures that the network produces a representation of the jet constituents respecting the Particle Cloud properties. It is made sure that the network's flavour predictions remain invariant under the permutation of jet constituents by applying a permutation invariant attention pooling followed by linear layers for classification. By analogy with graph structures, the attention mechanism can be interpreted similarly to the ones used in fully connected Graph Networks, with the attention scores playing a role similar to the edge features by capturing relationships within the jet structure.

After establishing the fundamental components of the utilised model's architecture, the foundational block forming the backbone of the model can be defined. This essential building block, referred to as the Heavy Flavour Transformer block (HFT), is structured in the following manner:

- The inputs are fed into a basic Multilayer Perceptron (MLP) layer followed by a ReLU activation function.

- The product of the MLP layer is then fed in an MHA layer before using a residual connection and layer normalisation.
- In addition to the MHA layer, a fully connected feed-forward layer is also added, identical to the original Transformer implementation [33] followed by a last residual connection and layer normalisation.

Unlike other Transformer models applied to jet (sub)structures, a *cls* token is not employed to embed the information of the jet structures into relevant features for classification. Instead, an attention pooling allowing is introduced, behaving similarly to a Max or Average pooling layer with an attention mechanism and learnable parameters. The attention pooling operates by employing an MLP projection layer, which enables local feature extraction. Subsequently, a softmax activation function is applied to calculate attention weights, allowing the layer to emphasise relevant elements in the sequence. The attention weights are then used to aggregate the sequence information by performing a weighted sum. To enhance the layer's performance, batch normalisation is applied to normalise, the ReLU [59] activation function is used to introduce non-linearity, and dropout regularisation is incorporated to prevent overfitting. The attention pooling layer can effectively capture essential information from the sequence and produce a condensed representation by incorporating these components that can be utilised for jet flavour classification. **DeepJetTransformer** could also be interpreted as a fully connected graph network using the jet's constituents as the nodes and the SDPA as a mechanism connecting all the node information for enhancing the feature engineering of the model.

#### 4.2.2 DeepJetTransformer Architecture

With all the components of **DeepJetTransformer** defined, the global structure of the model can be described. Figure 4 illustrates the detailed structure of **DeepJetTransformer**, which is as follows:

- The features of distinct jet constituents first undergo embedding via a series of three MLPs with output feature dimensions of (64, 128, 128), employing ReLU activation, residual connections, and batch normalisation. Dropout regularisation with a rate of 0.1 is applied following each batch normalisation operation.

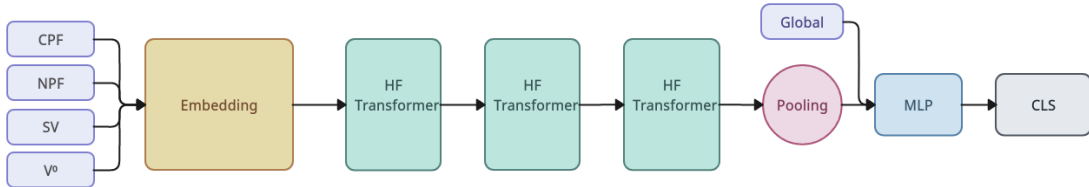


**Figure 4:** Schematic structure of **DeepJetTransformer** model.

- The resulting feature tensors are then concatenated to form a single tensor containing all the comprehensive information of the jet constituents.
- This global tensor is subsequently passed through three HFT blocks, each possessing a feature dimension of 128. Each block contains eight attention heads and incorporates a dropout rate of 0.1.
- The representation of the jet structure, obtained through the HFT blocks, is further condensed via attention pooling. The resulting tensor is concatenated with jet-level features, yielding a vector containing 135 relevant features for heavy flavour classification. Among these, 128 features originate from attention pooling, while the remaining seven variables represent the jet-level attributes.
- The jet representation is subsequently fed to three MLPs with output feature dimensions of (135, 135, 135), mirroring the structure of the input embedding MLPs.
- A single MLP followed by a SoftMax function is applied finally for classification.

#### 4.2.3 Training Methodology

PyTorch (v1.10.1) [60] was employed as the deep learning library in this study for the neural network model construction and the training process. The optimiser utilised was the Lookahead optimiser [61], with hyperparameters  $k = 6$  and  $\alpha = 0.5$  and a RAdam [62] as the base optimiser with a learning rate of 5e-3 and decay rates  $(\beta_1, \beta_2)$  set to (0.95, 0.999). The training was conducted over 70 epochs with a batch size of 4000, accompanied by a per-epoch linear learning rate decay starting after 70% of the training, gradually decreasing to 5e-5 by the final epoch. A cross-entropy loss function was used for optimisation. The training dataset comprised of 1 million jets, divided into an 80/20% train-validation split. Finally, the model was evaluated on a separate dataset of 1 million jets for performance assessment. Documentation for the sample preparation and training methodology, along with the relevant code, is publicly available here: [DeepJetFCC](https://github.com/Edler1/DeepJetFCC/tree/master/docs) <sup>1</sup>.

## 5 Classifier Performance

To evaluate the performance of **DeepJetTransformer**, clustered jets from  $Z \rightarrow q\bar{q}$  events at  $\sqrt{s} = 91.2$  GeV and  $Z(\rightarrow \nu\nu)H(\rightarrow q\bar{q})$  events at  $\sqrt{s} = 240$  GeV were considered. The emphasis was placed on the  $Z$  resonance for these studies, with the classification of  $H \rightarrow q\bar{q}$  events serving primarily as a comparison to the classification performance of other jet flavour taggers for future colliders, like **ParticleNetIDEA** [63, 64]. A binary classifier was constructed for each jet flavour  $q \equiv u, d, s, c, b, (g)$  with a signal flavour ( $i$ ) and a background flavour ( $j$ ):

$$S_{ij} = \frac{S_i}{S_i + S_j}, \quad (5.1)$$

where  $S_i$  are the softmaxed classifier outputs for  $Z \rightarrow q\bar{q}$  jets.

---

<sup>1</sup><https://github.com/Edler1/DeepJetFCC/tree/master/docs>

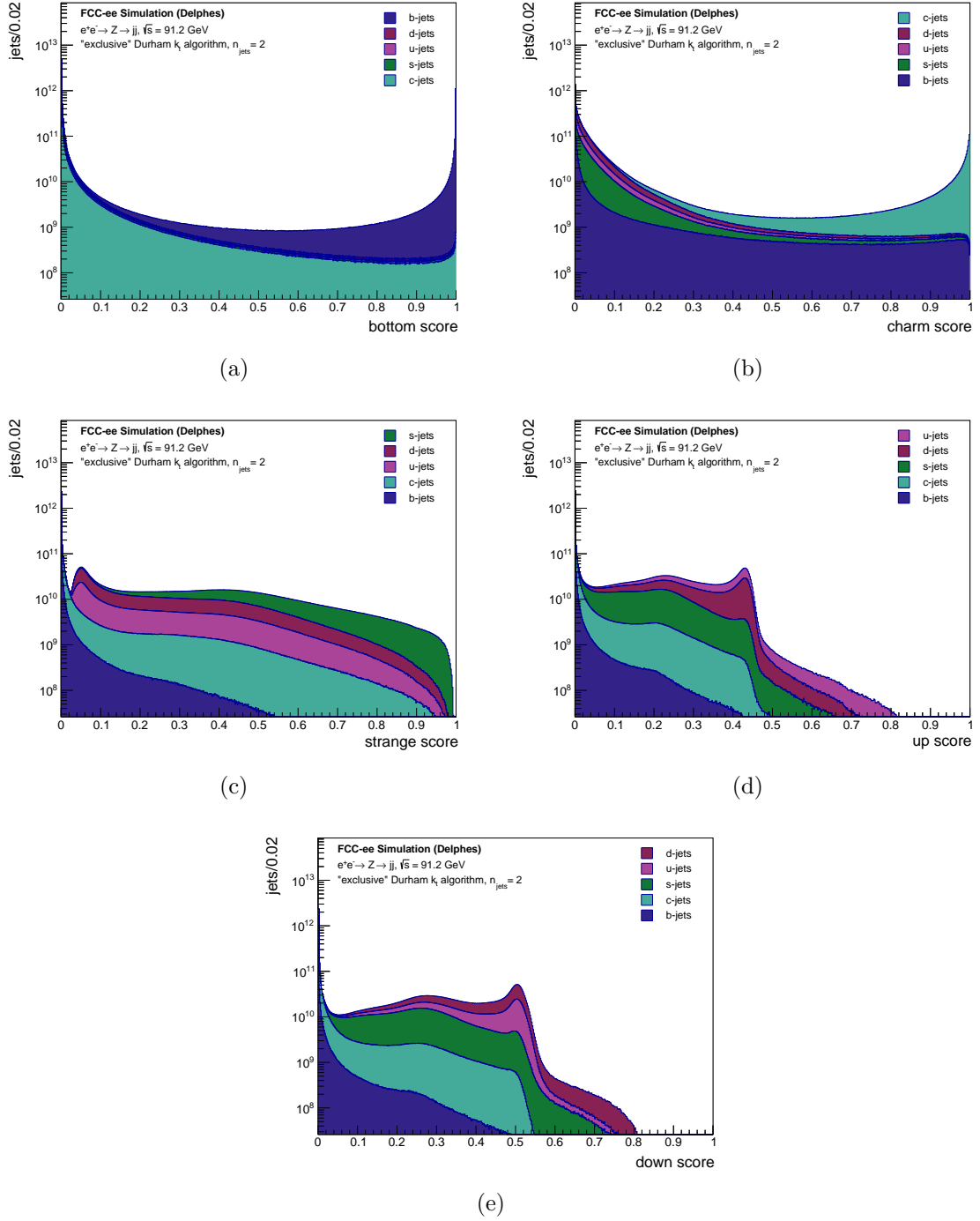


**Figure 5:** The softmaxed classifier scores of the five output nodes of `DeepJetTransformer` trained with clustered jets of  $e^+e^- \rightarrow Z \rightarrow q\bar{q}$  events at  $\sqrt{s} = 91.2$  GeV. The contributions of different MC flavours have been displayed.

These classifier scores of the five output nodes of `DeepJetTransformer` are shown in Figure 5. ROC curves were computed for each  $S_{ij}$  combination and are depicted in Figure

6 for the  $Z$  resonance and the  $ZH$  training. Predictably, the strongest discrimination is between  $b$ -jets and light jets ( $u, d, s$ ) and is roughly equivalent for all three light jets. The dominant background is from  $c$ -jets, originating from the similarity of  $b$ - and  $c$ -jets with a single reconstructed SV. The discrimination of  $c$ -jets from the light and  $s$ -jets likewise cluster together, displaying a similar performance. Figure 6b shows that in the low purity regime of  $c$ -jets, light jets are found to be discriminated worse than  $b$ -jets before a turnover point at  $\epsilon_{sig}^c \approx 80\%$ , after which distinguishing light jets becomes considerably easier than  $b$ -jets. It is unclear precisely why this turnover occurs, but it can also be found in ParticleNetIDEA [63], and is likely related to  $c$ -jets with displaced vertices that mimic those of  $b$ -jets. The sub-leading background comes from  $s$ -jets, clustered at low to mid charm scores, as also evident in Figure 5b, possibly due to two reasons: the  $V^0$  for some  $s$ -jets can be misclassified as an SV, and no SVs can be reconstructed for a significant number of  $c$ -jets.

When  $s$ -jets are taken to be the signal, as shown in Figure 6c,  $c$ - and  $ud$ -jets present the most challenging backgrounds, with  $c$ -jets being easier to discriminate against at all signal purities. The  $c$ -jet background can come from jets where a charm hadron decays to a strange hadron, and only the  $V^0$  can be reconstructed, or a strange hadron carries excess momentum. Some discrimination against the dominant  $ud$ -jets background can be achieved at higher cuts on the strange score, owing to the  $K^\pm/\pi^\pm$  separation and  $V^0$  reconstruction. Finally, Figures 5d and 5e show that classification is most challenging for  $u$ - and  $d$ -jets. When  $u$ -jets are taken to be the signal, it can be seen that DeepJetTransformer learns to discriminate  $u$ - vs  $d$ -jets with a  $\epsilon_{sig}^u \approx 15\%$  at a  $\epsilon_{bkg} = 10\%$ , possibly due to jet charge, which is better than a random classifier, although not considerably.

While considering the performance for  $H(\rightarrow q\bar{q})$  jets, depicted as dashed lines in Figure 6, no clear trend can be observed. Slight degradation in performance can be observed in the case of  $b$  tagging, compared to  $Z \rightarrow q\bar{q}$  jets, particularly when  $c$ -jets are taken to be the background. The discrimination for  $c$ -jets vs light ( $u, d, s$ ) jets is found to perform relatively the best.

Figure 6e shows that the best quark-gluon discrimination can be achieved against the  $b$  quarks. This performance can be attributed to several discriminating variables, like jet-constituent multiplicity, constituent momentum distribution, etc., but is likely dominated by the presence or absence of reconstructed SVs. It is the most challenging to discriminate the  $s$  and the light quarks from gluons due to their similar jet composition. The prevalent discriminating variable is jet charge, the effect of which is also diluted by the presence of antiquarks and is inferred indirectly by DeepJetTransformer since it is not one of the input variables.

The tagging efficiency of DeepJetTransformer was evaluated for three cases:  $b$  vs  $c$  tagging,  $c$  vs  $s$  tagging,  $s$  vs  $ud$  tagging. Figure 7 shows the efficiency of DeepJetTransformer over the entire jet momentum range and the jet-axis polar angle ( $\theta$ ) range for all three cases for two working points. The efficiency for  $b$  vs  $c$  tagging and  $c$  vs  $s$  tagging is mostly uniform, showing a good performance for all jet momenta. Similarly, the performance is largely uniform over the  $\theta$  range for all three cases, degrading at the extremes due to jet constituents being lost by fiducial cuts.



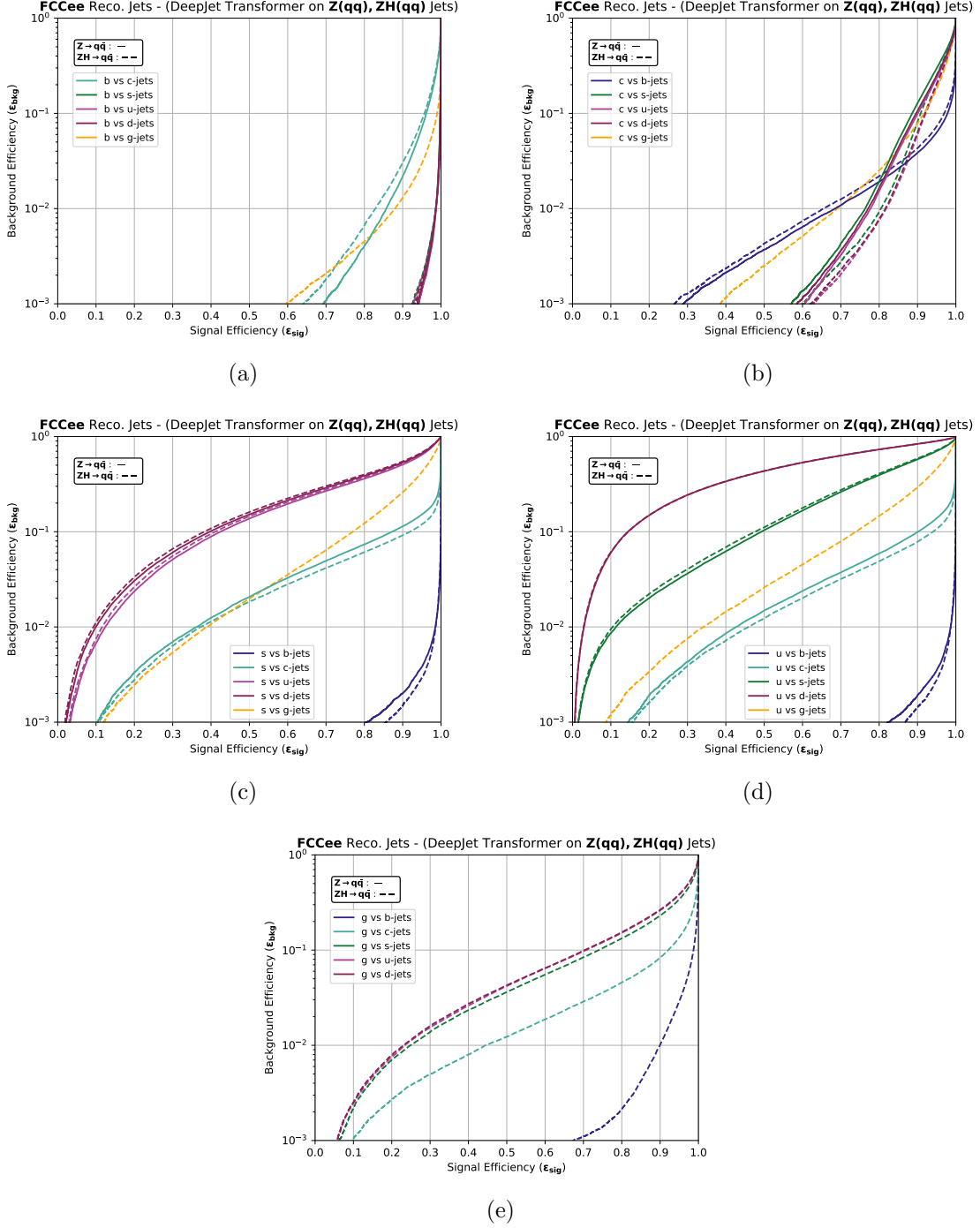


**Figure 6:** ROC curves for each  $S_{ij}$  combination, as defined in Eq. 5.1, where  $i$  is the signal parton flavour and  $j$  is the background flavour. The solid lines correspond to the classification of jets at the  $Z$  resonance at  $\sqrt{s} = 91.2$  GeV, while the dashed lines correspond to the classification of jets from  $Z(\rightarrow \nu\nu)H(\rightarrow q\bar{q})$  events at  $\sqrt{s} = 240$  GeV. No quark-gluon discrimination results are presented for jets from  $Z \rightarrow q\bar{q}$  events as the  $Z$  boson does not decay into gluons.

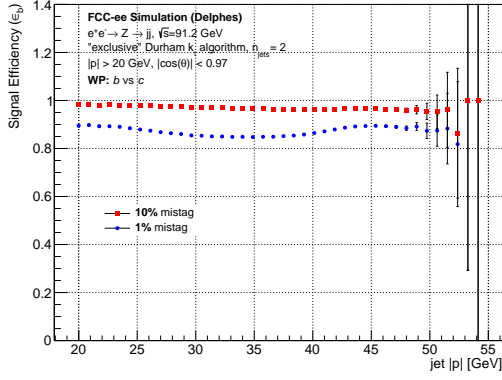
However, the  $s$  vs  $ud$  tagging efficiency displays a peculiar distribution over the momentum range of interest, as shown in Figure 7e. This was found to be dependent on the two most distinguishing features for identifying  $s$ -jets:  $K^\pm/\pi^\pm$  discrimination and  $V^0$  reconstruction. The low-momentum strange jets, on average, have lower  $K^\pm$  multiplicities, which leads to a reduced tagging efficiency. The very-low-momentum strange jets have a significantly low total charged-particle multiplicity, making  $V^0$  reconstruction crucial. The majority of such jets have a single reconstructed  $V^0$ , making it relatively easier to identify the  $s$ -jets. On the other hand, the low-momentum strange jets tend to have multiple  $V^0$ s, splitting the already low jet momentum among these  $V^0$ s and other hadrons. This is expected to make the strange jet identification more ambiguous. Hence, the  $s$ -tagging efficiency rises at very low momenta.

A similar but exaggerated trend in the distribution is seen for the looser working point of 10% mistag rate for jets with momentum values below 25 GeV. The efficiency is observed to be stable in momentum above this value. Some of this increase in  $s$ -tagging efficiency can be attributed to the fact that in jets with low particle multiplicities, the presence of a reconstructed  $V^0$  will have a very large effect on the likelihood that the jet is tagged as a strange jet. Another important aspect to note is that only a small fraction of jets ( $< 1\%$ ) with such very low momenta are present in  $Z$  boson decays. This means that these low-momentum jets will not have a large contribution to the training of the neural network or the working point determination, which will both be dominated by the bulk of the  $p$  distribution. The fact that the 10%  $u$ ,  $d$ -jet background efficiency also increases to 40% for momenta less than 25 GeV implies that this part of the jet momentum phase space is likely not optimally examined by the neural network. A potential method to improve would be to use flattened training weights and train on much larger samples with this part of the  $p$  distribution sufficiently populated. On the other hand, these jets contribute to a very small fraction of the total  $Z$  boson decays and the improvement in analyses requiring strange tagging would likely not be significant unless the physics case is specific.

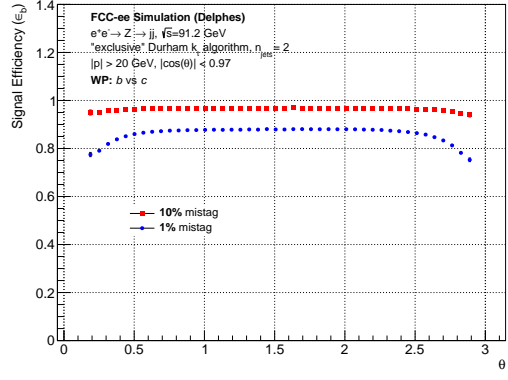
### 5.1 Qualitative Comparison with Other Taggers

A fair quantitative comparison with other taggers developed for future colliders is not feasible due to differing event samples and input features. However, the jet tagging performance trends are very similar to those of `ParticleNetIDEA` [63, 64]. The strange tagging efficiency of `ParticleNetIDEA` against the light jets surpasses that of `DeepJetTransformer`, owing to PID techniques like cluster counting and time-of-flight used by `ParticleNetIDEA` and the conservative PID estimates of `DeepJetTransformer`. A more detailed training dataset is expected to improve the tagging efficiencies of `DeepJetTransformer`. As one example, performance patterns, indicative of detector design impact, can already be assessed in case of strange tagging with the inclusion of a simple  $K^\pm/\pi^\pm$  classifier while achieving reasonably good tagging efficiencies. The inclusion of  $V^0$ s facilitates the exploration of another dimension of the detector design through the effects of the vertex and tracking detectors.

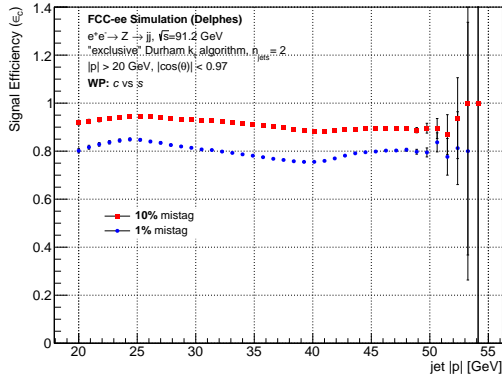
`DeepJetTransformer` outperforms `ParticleNetIDEA` in bottom-gluon discrimination, especially for efficiencies lower than 90%. `DeepJetTransformer` also has a



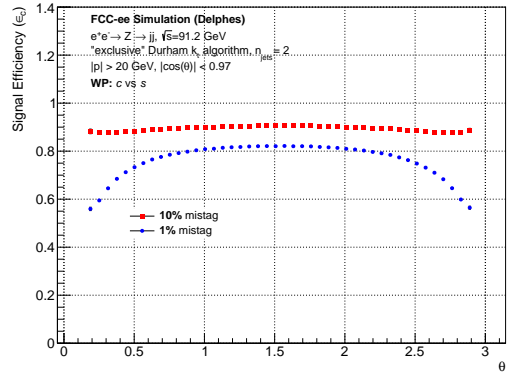
(a)  $b$  vs  $c$



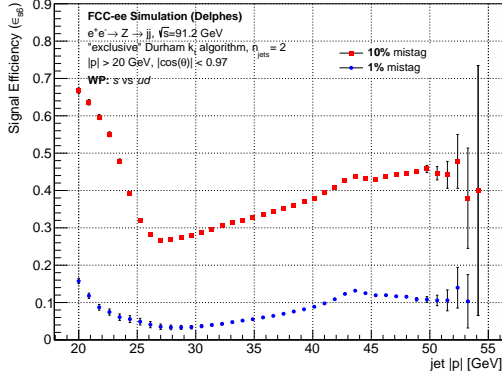
(b)  $b$  vs  $c$



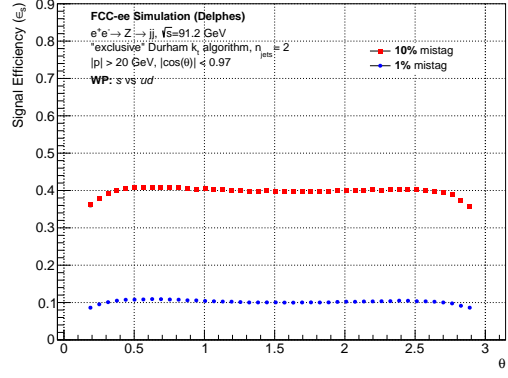
(c)  $c$  vs  $s$



(d)  $c$  vs  $s$



(e)  $s$  vs  $ud$



(f)  $s$  vs  $ud$

**Figure 7:** The jet flavour tagging efficiency over the range of jet momentum and the jet axis polar angle for jets of  $e^+e^- \rightarrow Z \rightarrow q\bar{q}$  events at  $\sqrt{s} = 91.2$  GeV. Three cases at 1% and 10% background efficiencies are shown:  $b$  vs  $c$  tagging,  $c$  vs  $s$  tagging,  $s$  vs  $ud$  tagging.

better discrimination of  $b$ -jet background for all other signal jet flavours. This efficient discrimination can be attributed to the inclusion of SVs.

With about  $10^6$  parameters and efficient transformer blocks as the workhorse, training `DeepJetTransformer` takes only 2 hours of training to converge after approximately 50 epochs on an NVIDIA Tesla V100s GPU. The computational investment of training is considerably less than the competing architectures, making it an excellent choice to study the constantly evolving detector designs efficiently.

## 5.2 Dependence on the Quality of Particle Identification

The discrimination of  $s$ -jets is widely regarded as one of the most challenging types of jet discrimination. Thus, it has received considerably less attention than its heavy-flavour counterparts, or indeed gluon discrimination. At the core of the problem is the fact that unlike in the discrimination of quarks vs gluons, which relies heavily on properties following from their differing colour factors  $C_F = 4/3$  vs  $C_A = 3$ , or heavy flavour tagging, which relies on displaced vertices of  $b/c$  hadrons, strange quarks are treated democratically by QCD and Electroweak theory prior to their decay. Discriminating strange and down jets is particularly challenging due to the same fractional charge of the initiating quarks. In practice, however, strange hadrons carry an excess of the scalar summed momentum of strange jets. This idea was also explored in the context of hadron colliders [25]. In this work, we exploit the excess momentum carried by strange hadrons, firstly through the inclusion of  $V^0$  variables and secondly through  $K^\pm/\pi^\pm$  discrimination.

The  $K^\pm$  classification scenarios were defined by fixing the efficiency of misidentification to  $\pi^\pm$  and varying the  $K^\pm$  identification efficiency. In addition, the limiting cases of Kaon identification with 0% and 100% efficiencies were considered. These are referred to henceforth as the no  $K^\pm$ ID and the perfect  $K^\pm$ ID scenarios. The considered efficiencies and the misidentification rates are the following:

$K^\pm$ ID efficiency	0%	20%	40%	60%	80%	90%	95%	100%
$\pi^\pm$ misID efficiency	0%	10%	10%	10%	10%	10%	10%	0%

**Table 5:** Considered scenarios for  $K^\pm$  and  $\pi^\pm$  particle identification performance.

The largest performance gain with the addition of  $K^\pm$ ID information is predictably in the classification of  $s$  vs  $ud$  jets, shown in Figure 8. Using the no  $K^\pm$ ID scenario as a reference, with a  $\epsilon_{sig}$  of 31.6% at a  $\epsilon_{bkg}$  of 10%, strange tagging efficiency improvements of 11.4%, 25.9%, and 32.9% are evident as the  $K^\pm$ ID efficiency is increased to 60%, 90%, and 95%, respectively. The perfect  $K^\pm$ ID scenario shows the most sizeable performance gain in  $\epsilon_{sig}$  of 82.9%. This large performance improvement over the 95%  $K^\pm$ ID efficiency with the efficiency of misidentification to  $\pi^\pm$  of 10% scenario suggests that minimising this misidentification is crucial to strange jet tagging, given their high  $\pi^\pm$  multiplicity [25].

The performance gain for other forms of classification was marginal, with the exception of  $c$  vs  $ud$  and  $u$  vs  $d$  discrimination. For  $c$  vs  $ud$ , a performance gain of 1.8% from a  $\epsilon_{sig}$  of 89.3% to 90.9% at a  $\epsilon_{bkg}$  of 10% is observed while comparing the no  $K^\pm$ ID and the perfect  $K^\pm$ ID scenarios. In the case of  $u$  vs  $d$ , a 12.5% performance gain from a  $\epsilon_{sig}$  of 13.6% to 15.3% at a  $\epsilon_{bkg}$  of 10% is observed.

These results indicate the importance and necessity of particle identification techniques, especially for strange quark studies. Such methods are already being explored, like cluster counting and time-of-flight, as foreseen for IDEA [65], and compact-Ring Imaging CHerenkov (RICH) detectors, as being studied for another detector concept for FCC-ee, CLD [66] and ILD, the detector concept developed for ILC [14].

### 5.3 Dependence on the Presence of Neutral Kaons

Another distinguishing feature of strange jets is an excess of leading  $V^0$ s, reconstructed  $K_S^0$  and  $\Lambda^0$ . As noted earlier, these are expected to be more significant in the scarcity of charged Kaons. The inclusion of  $V^0$  variables, as Figure 8 shows, results in an improvement of signal efficiency ranging from 16.4% in case of no  $K^\pm$ ID to 4.5% in the case of perfect  $K^\pm$ ID at a background efficiency of 10% for  $s$  vs  $ud$  discrimination. This trend proves the importance of  $V^0$ s to identify strange jets with low  $K^\pm$  multiplicities or substandard  $K^\pm/\pi^\pm$  discrimination. The performance gain in other forms of classification was again marginal.

A low-material vertex detector with extremely high spatial resolution and a light tracker with numerous measurement points are essential for an accurate track and vertex reconstruction. These, in turn, affect the precise reconstruction and identification of the  $V^0$ s.

### 5.4 Importance of Variable Classes and Individual Variables

Aiming to estimate the relative importance of a given variable class (e.g. SV variables), the classifier performance was evaluated using the Permutation Feature Importance [67, 68] method. In particular, the variable class under investigation was shuffled amongst all other jets, keeping the rest of the variables unchanged. The performance change concerning  $b$  vs  $c$ ,  $c$  vs  $s$ , and  $s$  vs  $ud$  jet discrimination was considered with respect to the baseline, where no variable classes were shuffled. Charged jet constituent variables, listed in Table 3, were

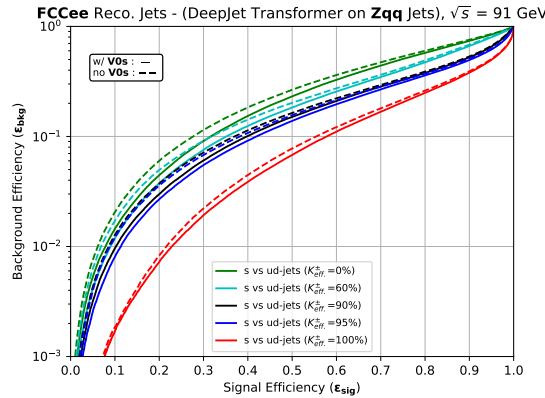


**Figure 8:** The dependence of strange jet tagging performance on the inclusion of  $V^0$ s and charged Kaon identification scenarios.

found to be the most impactful variable class for all types of discrimination at a background efficiency of  $\epsilon_{bkg} = 10\%$ , as depicted in Table 6. This is presumably due to charged particles being the majority of the reconstructed particles in the jets. SV variables, listed in Table 4, primarily benefited  $c$  vs  $s$  discrimination, with  $s$  vs  $ud$  tagging particularly insensitive. Of the remaining three variable classes,  $V^0$  variables and neutral jet constituent variables were found to almost exclusively impact the performance of  $s$  vs  $ud$  discrimination, with little impact on both  $b$  vs  $c$  and  $c$  vs  $s$  discrimination, justifying the inclusion of  $V^0$ s for identifying  $s$ -jets through conservation of strangeness. Jet-level variables were found to be the least significant, marginally impacting  $s$  vs  $ud$  discrimination, and having virtually no impact on heavy flavour discrimination. Moving to the high purity regime at a background efficiency of  $\epsilon_{bkg} = 0.1\%$ , primarily the same trends were observed, with the impact of any variable type being amplified. SV variables, in particular, became hugely important to heavy flavour tagging, reaching almost equal in impact to the charged jet constituent variables, proving that the presence and properties of SVs are definitive indicators for identifying heavy flavour jets.

Variable Class		Jet-level	Charged	Neutral	SV	$V^0$
$\epsilon_{bkg} = 10\%$	$b$ vs $c$	2.4%	62.4%	2.2%	13.9%	0.1%
	$c$ vs $s$	1.2%	65.7%	2.9%	29.6%	0.2%
	$s$ vs $ud$	7.6%	59.4%	21.8%	5.0%	16.4%
$\epsilon_{bkg} = 0.1\%$	$b$ vs $c$	6.6%	97.0%	8.0%	89.9%	0.6%
	$c$ vs $s$	9.3%	96.1%	11.0%	77.9%	0.2%
	$s$ vs $ud$	35.9%	91.0%	57.3%	7.4%	43.8%

**Table 6:** Performance decrease in signal efficiency ( $\epsilon_{sig}$ ) after permutation of variable classes defined in Section 4.1 for fixed background efficiencies ( $\epsilon_{bkg}$ ) of 10% and 0.1%.

The above studies were repeated to estimate the relative importance of individual variables (e.g.  $m^{SV}$ ), where rather than shuffling an entire variable class amongst jets, one individual variable was shuffled amongst itself. The 64 variables can be loosely split into the following categories:

- Kinematic ( $|p|$ ,  $E$ ,  $p/p_{jet.}$ ,  $\theta$ ,  $\Delta\theta$ , ...)
- PID ( $isPhoton$ ,  $K^\pm ID$ , ...)
- Track ( $D_0$ ,  $z_0$ , ...)

It was found that, at a background efficiency of 10%, kinematic variables of charged particle constituents, including  $\frac{E_{ch.}}{E_{jet}}$  and  $\frac{|p_{ch.}|}{|p_{jet}|}$ , were generally impactful, particularly for  $c$  vs  $s$  discrimination. Track variables, such as  $D_0/\sigma_{D_0}$  and  $z_0$ , were the most impactful, though less for  $b$  vs  $c$  than other types of discrimination, possibly due to their redundant information after the inclusion of SVs. PID variables had little impact on  $b$  vs  $c$  and  $c$  vs  $s$  discrimination, but  $K^\pm ID$  and photon ID were the most important for  $s$  vs  $ud$  discrimination, as was observed earlier. The high purity regime at a background efficiency

of 0.1% resulted in similar trends, though with PID variables, including  $K^\pm\text{ID}$  and photon ID, decreasing in importance and being somewhat replaced by kinematic ones. It should be stated that the baseline  $K^\pm\text{ID}$  scenario, as mentioned in Section 5, is deliberately pessimistic, which could account for its decrease in importance. Track variables remained the most impactful. The secondary vertex mass  $m^{\text{SV}}$  became the most impactful variable in  $b$  vs  $c$  discrimination at high purity by a sizeable margin, as SV kinematics store essential information about the decaying hadrons. The results of this study are summarised in Table 7 below.

Variable		$\ln(E_{\text{ch.}})$	isPhoton	$K^\pm\text{ID}$	$m^{\text{SV}}$	$p^{V^0}$	$z_0$	$D_0/\sigma_{D_0}$
$\epsilon_{bkg} = 10\%$	$b$ vs $c$	3.5%	0.3%	0.2%	3.0%	0.1%	7.8%	11.6%
	$c$ vs $s$	23.8%	0.7%	0.5%	0.3%	0.2%	20.9%	39.1%
	$s$ vs $ud$	12.8%	16.6%	38.8%	0.0%	9.2%	23.3%	26.7%
$\epsilon_{bkg} = 0.1\%$	$b$ vs $c$	13.8%	1.3%	0.9%	67.2%	0.8%	34.1%	45.0%
	$c$ vs $s$	57.6%	0.9%	4.8%	7.0%	0.3%	56.2%	79.5%
	$s$ vs $ud$	35.0%	28.0%	59.0%	0.4%	34.7%	60.5%	80.1%

**Table 7:** Performance decrease in signal efficiency ( $\epsilon_{sig}$ ) after permutation of individual variables defined in Section 4.1 for fixed background efficiencies ( $\epsilon_{bkg}$ ) of 10% and 0.1%. A set of seven variables, chosen among the most impactful, is presented here.

## 5.5 Dependence on the Flavour Definition

Defining the flavour of a reconstructed jet is a complex task. Several definitions have been used in past and current experiments to assign the flavour of MC-generated jets, reconstructed using a detector simulation. However, flavour definitions designed for jets clustered with cone-shaped algorithms, like the anti- $k_T$  algorithm [44], are not suitable for irregularly-shaped jets, like the ones clustered in this study with the exclusive (Durham)  $e^+e^- k_T$  algorithm [42].

Various flavour definitions were considered to study their impact on the classifier performance for  $Z$  boson decay events. For conciseness, a comparison of two of these definitions is reported here. The first of these is the Ghost Matching algorithm [69] used at CMS, which defines the flavour of a jet by finding the hadrons or partons from the MC history of the jet, called ghosts, clustered with the jet after scaling their momentum with a minuscule factor. The other definition assigns the flavour of a jet as the flavour of the quark to which the  $Z$  boson decays. A performance difference of 11.8% was seen in the discrimination of  $s$ -jets vs  $ud$ -jets at a fixed background efficiency of 10% between the two flavour definitions. Such a significant difference makes the considered jet flavour definition consequential while comparing different classifiers.

## 6 Example of Performance: The $Z$ Boson at the FCC-ee

The  $Z$  boson decays relatively uniformly to the five quark flavours, and none of the decay channels to  $q\bar{q}$  pairs are suppressed. Thus, tagging a particular jet flavour entails



discrimination against every other flavour. Especially, isolating  $Z \rightarrow s\bar{s}$  events from the exclusive decays of the  $Z$  boson provides a challenging case to tag the  $s$ -jets by eliminating both the heavy jets and the light jets. The dominant discriminating variable against the heavy jets is the reconstructed SVs, while it is the presence of a leading strange hadron against the light jets. This makes tagging  $Z \rightarrow s\bar{s}$  events an ideal metric to assess the performance of **DeepJetTransformer** and allows for a unique opportunity to access a hitherto scarcely studied channel.

### 6.1 Physics Potential at the $Z$ Resonance

After the discovery of the  $Z$  boson at the Super Proton Synchrotron (SPS) at CERN in 1983 [70, 71], this neutral vector boson was extensively studied at the LEP collider and the SLAC Linear Collider. The existence of the  $Z$  boson confirmed the electroweak mixing [72, 73] and the measurement of its width constrained the number of neutrino generations to three [74–78].

Heavy-flavour tagging was performed at LEP [16, 17] and the Tevatron [18, 19] by reconstructing SVs and exploiting these to remove the background from light-flavour jets. SLD also tagged  $Z \rightarrow s\bar{s}$  events, to measure  $A_s$ , by the absence of reconstructed  $B$  and  $D$  hadrons and the presence of  $K^\pm$  or  $K_S^0$  [79]. The particle identification was performed at SLD, as at DELPHI, with a RICH detector [80, 81]. At most other detectors,  $dE/dx$  was used for PID [82, 83], with the addition of timing at ALEPH [84].

The proposed FCC-ee program provides a unique opportunity to push the  $Z$  boson measurements to their ultimate limit. The four-year-long FCC-ee run at and around the  $Z$  resonance will produce an unprecedented  $6 \times 10^{12}$  total decays. The integrated luminosity expected at the  $Z$  resonance at FCC-ee is  $125 \text{ ab}^{-1}$ , about  $10^6$  times that of LEP. The statistical errors on the mass and width of the  $Z$  boson can be reduced from 1.2 MeV and 2 MeV to 5 KeV and 8 KeV [4], respectively. Lower center-of-mass energy spread due to beam energy calibration will benefit in reducing the systematic uncertainty of these quantities. Measuring the forward-backward and polarisation asymmetries is a powerful method to estimate the effective weak mixing angle,  $\sin^2 \theta_W^{\text{eff}}$ , for which the statistical uncertainty is expected to reduce to about  $10^{-6}$ , corresponding a more than thirty-fold improvement [4].

Studying the hadronic decay channels of the  $Z$  boson is a very important aspect of the FCC-ee physics program. The couplings and decay widths of the  $Z$  boson have only been measured to the heavier quarks,  $b$  and  $c$ . The only study of the  $s$  quark decay of the  $Z$  boson available in the literature is preliminary [85]. For the lighter quarks,  $s$ ,  $u$ , and  $d$ , these properties are typically only listed collectively for up-type and down-type quarks [53]. Similarly, the axial and vector couplings have also been collectively measured for up-type and down-type quarks [53].

Future colliders with a dedicated  $Z$  boson run, like FCC-ee, will improve the precision of all these measurements, making the lighter quarks accessible. Individual measurements of the quark vector and axial couplings should be possible via their forward-backward asymmetries, corresponding partial decay widths of the  $Z$  boson, and the precise knowledge of  $A_e$ . The experimental systematic uncertainties corresponding to these measurements are also expected to drastically improve due to better detector designs with PID and vertexing



[4]. This section aims to evaluate the performance of `DeepJetTransformer` in tagging  $Z \rightarrow q\bar{q}$  events. This will be demonstrated by isolating  $Z \rightarrow s\bar{s}$  events from the exclusive hadronic decays of the  $Z$  boson in the FCC-ee environment. Further backgrounds are not considered.

## 6.2 Event and Jet Selection

The simulated samples described in Sec. 2.3 are used. These samples use `Pythia8.303` [41] to generate  $e^+e^- \rightarrow Z \rightarrow q\bar{q}$  events, where  $q \equiv b, c, (u, d, s)$ , at the center-of-mass energy of 91.2 GeV and were clustered exclusively into 2 jets with `FastJet-3.3.4` [42] using the  $e^+e^-$   $k_T$  algorithm [43].

Events are selected if exactly two jets could be reconstructed with their final constituents. Jets with low momentum or jet axes outside the fiducial region of the detector are excluded. An event is selected if both of its jets have a momentum magnitude ( $|p|$ ) greater than 20 GeV and the polar angle ( $\theta$ ) of their jet axes within 14 and 176 degrees. Events are required to have jets of the same MC flavour, defined as the flavour of the quarks to which the  $Z$  boson decays.

## 6.3 Performance and Working Points

All jets from  $Z \rightarrow q\bar{q}$  events are independently evaluated using `DeepJetTransformer`. Discriminants are defined to sequentially remove the heavy flavour background ( $b$ - and  $c$ -jets) and the light flavour background ( $u$ - and  $d$ -jets). The  $s$ -jets are first tagged to be discriminated from  $b$ - and  $c$ -jets by defining the discriminant as in Eq. 5.1 with  $s$ -jets as signal and  $b$ - and  $c$ -jets as background. For the jets tagged by introducing a cut on this discriminant, another discriminant is defined to distinguish  $s$ -jets from  $u$ - and  $d$ -jets through the same method. The signal efficiencies after each subsequent cut, corresponding to four working points with increasing purity, are reported in Table 8.

As shown in Table 8, the working points are defined for four different sets of misidentification rates, referred to as mistag rates. Working Point 1 (WP1) corresponds to a mistag rate of 10% while tagging  $s$ -jets versus the background of  $b$ - and  $c$ -jets and a mistag rate of 10% while tagging  $s$ -jets versus the background of  $u$ - and  $d$ -jets. Working Point 2 (WP2) corresponds to a stricter mistag rate of 1% while tagging  $s$ -jets versus the background of  $b$ - and  $c$ -jets, keeping the mistag rate the same as WP1 while tagging  $s$ -jets versus the background of  $u$ - and  $d$ -jets. Both mistag rates are 1% for Working Point 3 (WP3). Working Point 4 (WP4) is the tightest scenario, with both mistag rates being 0.1%.

The  $Z$  boson resonance is reconstructed from the 4-momentum of the two jets. The reconstructed invariant dijet mass distribution, separated by the MC flavour of the resulting hadronic jets, is shown in Figure 9a. The hadrons in  $b$ -jets tend to have longer decay chains, which causes more momentum to be lost via neutrinos, resulting in a wider invariant mass distribution for  $Z \rightarrow b\bar{b}$ . Similarly, the  $Z \rightarrow c\bar{c}$  reconstructed invariant mass distribution also shows a tail, but for the lighter flavour jets,  $s$ ,  $u$ , and  $d$ , a clear Gaussian peak can be seen at the  $Z$  resonance.

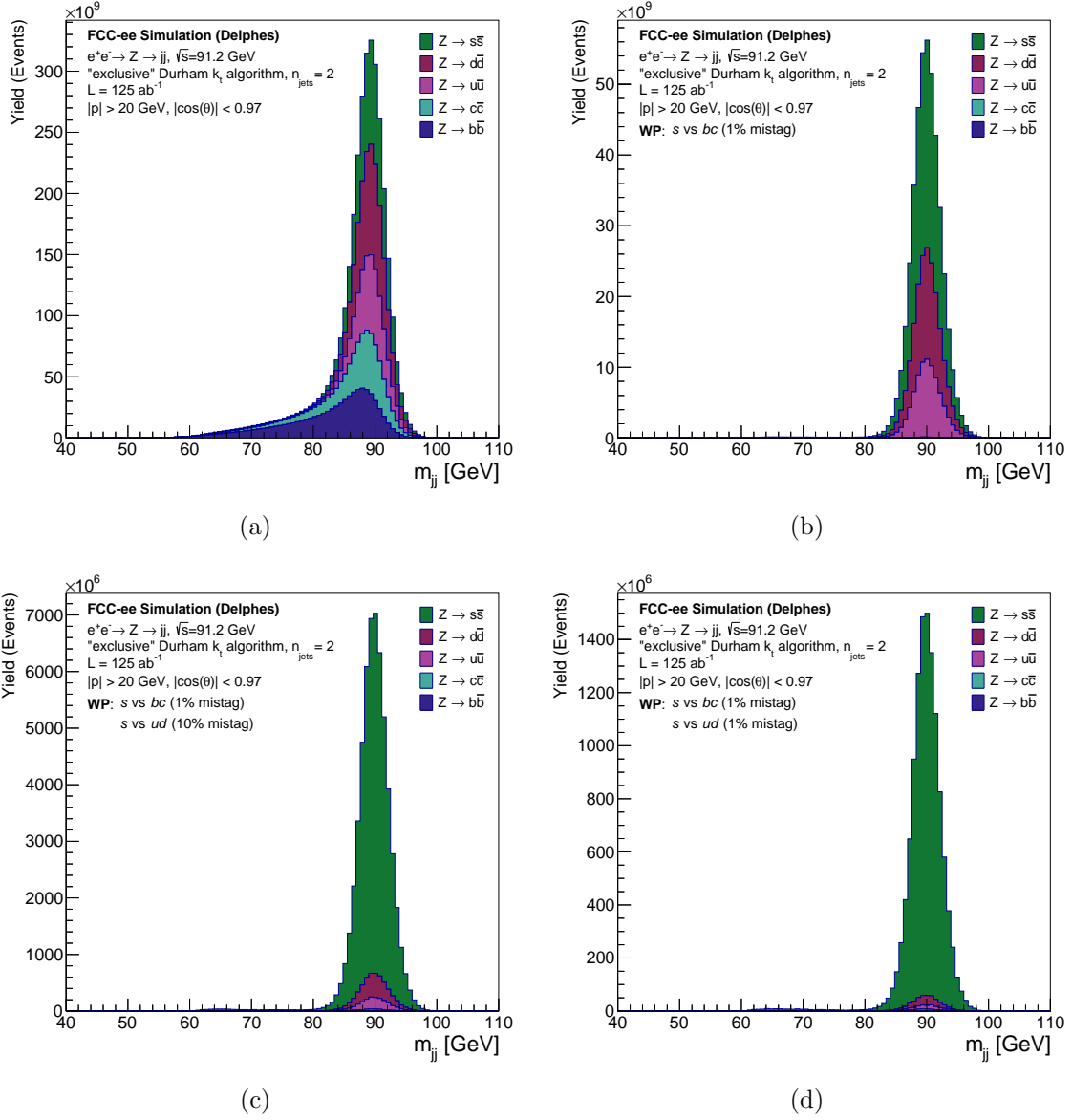


**Figure 9:** The reconstructed invariant mass of the dijet system before and after tagging both jets with DeepJetTransformer, corresponding to WP2 and WP3 in Table 8, for an assumed integrated luminosity of  $125 \text{ ab}^{-1}$ . Both jets are required to be tagged in each case. Shown are (a) the distribution without tagging applied, (b) after the rejection of  $b$ - and  $c$ -jets vs  $s$ -jets at 1% mistag rate, (c) the distribution after rejection of  $b$ - and  $c$ -jets at 1% and  $u$ - and  $d$ -jets vs  $s$ -jets at 10% mistag rate, (d) the distribution after rejection of  $b$ - and  $c$ -jets at 1% and  $u$ - and  $d$ -jets vs  $s$ -jets at 1% mistag rate.

		Mistag Rate [%]	Efficiency [%]	$N_{sig}$	$N_{bkg}$
<b>WP1</b>	$s$ vs $bc$	10	$98.93 \pm 0.03$	$7.35 \times 10^{11}$	$1.35 \times 10^{12}$
	$s$ vs $ud$	10	$40.03 \pm 0.04$	$1.45 \times 10^{11}$	$3.25 \times 10^{10}$
<b>WP2</b>	$s$ vs $bc$	1	$54.18 \pm 0.04$	$2.38 \times 10^{11}$	$2.06 \times 10^{11}$
	$s$ vs $ud$	10	$39.28 \pm 0.06$	$5.10 \times 10^{10}$	$5.57 \times 10^9$
<b>WP3</b>	$s$ vs $bc$	1	$54.18 \pm 0.04$	$2.38 \times 10^{11}$	$2.06 \times 10^{11}$
	$s$ vs $ud$	1	$10.05 \pm 0.11$	$1.12 \times 10^{10}$	$4.77 \times 10^8$
<b>WP4</b>	$s$ vs $bc$	0.1	$17.96 \pm 0.06$	$3.23 \times 10^{10}$	$6.98 \times 10^9$
	$s$ vs $ud$	0.1	$1.98 \pm 0.33$	$3.56 \times 10^8$	$3.38 \times 10^6$

**Table 8:** Presented are the efficiencies to select  $s$  quark jets and the mistag rate for other flavours at four different working points. Also listed are the expected yields calculated for an integrated luminosity of  $125 \text{ ab}^{-1}$ . Signal is defined as  $Z \rightarrow s\bar{s}$  events while the background is composed of  $Z \rightarrow q\bar{q}$  events (all quarks but  $s$  quarks) events. The number of observed events is significantly above the canonical discovery significance of five standard deviations for all selections.

These jets are first tagged to remove the background of  $b$ - and  $c$ -jets by defining the discriminant, as described above. If both jets from a  $Z$  boson decay event are tagged with the same flavour, they are used to reconstruct the invariant mass. The distribution of this invariant mass after the first tag is displayed in Figure 9b, with the contributions of the MC flavours of the jets indicated. The events passing the anti- $b/c$  tag requirement are subsequently tagged with the  $s$  vs light quark tagger to remove the background of  $u$ - and  $d$ -jets. Figures 9c and 9d show the distribution of the reconstructed invariant mass of  $Z$  boson. Both jets are required to be tagged in each stage of the selection.

The reconstructed tagged  $Z$  resonance in Figure 9 shows that the  $Z \rightarrow s\bar{s}$  sample is extremely pure after requiring two tags. Similarly, Table 8 lists events corresponding to an integrated luminosity of  $125 \text{ ab}^{-1}$  that are significantly above the canonical discovery

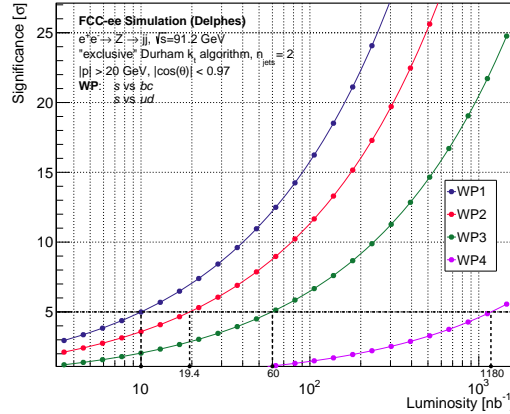


**Figure 10:** Discovery Significance vs Luminosity for all Working Points

significance of  $5\sigma$ . It is important to realise that machine backgrounds and irreducible backgrounds from other standard model processes are not considered in this study. However, the remarkable sensitivity warrants investigation of how limited the integrated luminosity needs to be to observe  $Z \rightarrow s\bar{s}$  in the considered scenario. Figure 10 shows the discovery significance of the process  $Z \rightarrow s\bar{s}$ , under the background-free scenario, as a function of integrated luminosity. The discovery significance,  $Z$ , in  $\sigma$ , is defined [86] as,

$$Z = \sqrt{2 \left[ (N_{sig} + N_{bkg}) \log \left( 1 + \frac{N_{sig}}{N_{bkg}} \right) - N_{sig} \right]}. \quad (6.1)$$

$N_{sig}$  and  $N_{bkg}$  refer to the number of signal and background events, respectively. Their corresponding values at each working point can be referred to from Table 8. It can be seen that a  $5\sigma$  significance can be achieved with minuscule luminosities compared to the FCC-ee run plan, even at the tightest working point. For WP3, corresponding to Figure 9, a  $5\sigma$  significance can be reached with a luminosity of  $60 \text{ nb}^{-1}$ , equivalent to *less than a second* of the FCC-ee run at the  $Z$  resonance.

These findings will open up avenues at FCC-ee for measurements that require ultra-pure  $Z \rightarrow q\bar{q}$  samples, at least for the three heaviest flavours to which the  $Z$  boson decays. Some examples are vector and axial couplings of the  $Z$  to up- and down-type quarks and possibly even individual quark flavours and asymmetry parameters of the  $Z$  boson in the hadronic decay channels. LEP and SLD performed comprehensive measurements of the forward-backwards charge asymmetry for  $e^+e^- \rightarrow b\bar{b}$  [53], similar precise measurements for the charm and the strange quark, and possibly the light quarks, will become feasible at the FCC-ee.

## 7 Outlook

The current input feature set is likely far from optimal and could be extended to incorporate further parameters, including those related to jet-shape variables or the full covariance matrix. A primary focus would be to include more realistic PID assumptions based on a specific detector scenario. In Ref. [63], for instance, the mass calculated from the time-of-flight ( $m_{t.o.f.}$ ) and the number of primary ionisation clusters along the track ( $dN/dx$ ) are directly fed as inputs to the NN. On the other hand, it is also evident from the feature importance studies that there is some overlap in the current feature set, which could likely be reduced with marginal impact on the discriminative performance, thus lowering computational complexity if paired with a simplified architecture.

There is also significant room for hyperparameter tuning. The used batch size of 4000 is comparatively large, with typical values being less than 1024. The large batch size was chosen for training stability but has been shown to potentially lead to poorer generalisation. The chosen number of training jets of  $O(10^6)$  can be considered a rough lower bound given the number of parameters in the network  $\sim 10^6$ . A natural next step would be to train the network on a much larger number of jets. Further improvements in the network architecture are likely, though this was not explored in the context of these studies.

Subdividing jet flavours into categories with unique signatures, such as  $b$ -jets into those that decay hadronically and semi-leptonically, or  $g \rightarrow b\bar{b}$  splittings that do not resemble the typical radiation pattern of a gluon jet, is likely to improve discrimination performance. Additional categories could likewise be included for anti-quarks, which would be helpful in discriminating dijet events where a quark-antiquark pair is expected, such as in  $Z \rightarrow s\bar{s}$  decays. More generally, much could be gained from event-level tagging, particularly for  $s$  quark jets, where discrimination comes primarily from a hard Kaon. Tagging an entire event could require not only a hard Kaon in one jet, but a hard Kaon of the opposite flavour in the other, thus discriminating against Kaons produced during the dressing of a light quark.

The updated design of the IDEA detector concept has the innermost layer of the vertex detector at 1.2 mm instead of 1.7 mm. It will improve the impact parameter resolution and, consequently, the displaced vertex resolutions, thus enhancing the performance of heavy flavour tagging. Further improvement is expected from an ultra-light ALICE ITS3-like vertex detector [87]. An updated version of CLD [66] is being developed with a dedicated RICH PID detector, ARC, which is expected to aid in strange tagging.

A natural extension of isolating  $Z \rightarrow s\bar{s}$  events would be to measure the branching fraction and coupling of the  $Z$  boson to the  $s$  quark and assess further flavour-dependent properties at the  $Z$  pole that are sensitive to extensions of the standard model. Extrapolating the excellent performance of **DeepJetTransformer** in discriminating strange jets and the continuing improvement of jet flavour taggers along with more sophisticated inputs, there is clear potential for the precise study of the light  $u$  and  $d$  quarks at the  $Z$  resonance at the FCC-ee.

The similar performance in Higgsstrahlung events suggests the opportunity to measure the Yukawa coupling of the  $s$  quark, and the decent gluon discrimination, especially against heavy quarks, will make gluon final states accessible as well. The much larger  $Z$  boson cross-section will also provide opportunities for calibration and performance validation on data before the Higgs boson decay to  $s$  quarks is examined, which is likely to reduce experimental uncertainties.

## 8 Conclusion

Deep learning techniques have shown great potential in analysing complex jet structures and extracting subtle flavour signatures in jet flavour identification. The transformer-based model presented in this work can be trained considerably more quickly compared to the state-of-the-art graph neural network-based taggers, making it uniquely suited for prospective studies of the developing detector concepts. The discrimination power of this framework called **DeepJetTransformer** is presented for FCC-ee, allowing the classification of all jet flavours in  $e^+e^-$  collisions at the  $Z$  resonance. It should be noted that even though this study focuses on FCC-ee and the IDEA detector, the conclusions are general, and **DeepJetTransformer** can also be utilised at other collider projects with appropriate adjustments.

A tagging efficiency for  $b$ -jets of about 99% can be achieved against  $s$ ,  $u$ , and  $d$  jets at a background efficiency of 0.1%, pointing to an excellent  $b$ -jet discrimination, dominantly owing to the secondary vertex reconstruction coming from the expected excellent detector resolution. A  $c$ -jet tagging efficiency of about 90%(70%) can be achieved when discriminating from  $b$ -jets, at a background efficiency of 10%(1%).

Excellent discrimination can be achieved for  $s$ -quark tagging against the  $b$ - and  $c$ -quark jet background. Against the most challenging background of light jets, a 40% efficiency for  $s$  quark jets can be achieved at a background efficiency of 10%. Some discrimination can be achieved even between  $u$ - and  $d$ -jets. The performance is partially attributed to the inclusion of  $V^0$ s. Another significant performance enhancement is seen when  $K^\pm/\pi^\pm$  discrimination is included.

It is shown that  $Z \rightarrow s\bar{s}$  can be efficiently isolated from other hadronic decays of the  $Z$  boson. These results show that modern jet flavour tagging techniques can isolate very pure samples of light quark decays originating from vector bosons. We hope that light quark jet tagging will create opportunities for a new category of potential studies at future lepton colliders, including assessment of the feasibility of completely new or more precise measurements and enhancement of the sensitivity to new physics phenomena.

### Acknowledgments

We want to thank our CMS colleagues at the IIHE in Brussels, especially A.R. Sahasransu and Lode Vanhecke for their preparatory work, and Emil Bols for their valuable discussions regarding **DeepJetTransformer**. We would also like to thank Kyle Cormier at the UZH for helpful discussions regarding the feature importance studies.

This project is supported by the European Union’s Horizon 2020 research and innovation programme under grant agreement No 951754. Kunal Gautam and Eduardo Ploerer are supported by FWO (Belgium) and SNF (Switzerland). Freya Blekman acknowledges support from DESY (Hamburg, Germany), a member of the Helmholtz Association HGF, and support by the Deutsche Forschungsgemeinschaft (DFG, German Research Foundation) under Germany’s Excellence Strategy – EXC 2121 ”Quantum Universe” – 390833306. Armin Ilg is supported by SNF in Switzerland.

### Author Contribution

KG implemented and AI tested the vertex reconstruction algorithm. ADM designed and implemented the **DeepJetTransformer** architecture. EP adopted the model for the FCC-ee environment, performed input feature selection, and trained and evaluated the performance for several scenarios. KG assessed the classifier performance by isolating  $Z \rightarrow s\bar{s}$  events from the exclusive  $Z \rightarrow q\bar{q}$  decays. FB and AI supervised and reviewed the work throughout the study. FB, ADM, KG, AI, and EP contributed to the writing and editing of this paper.

## References

- [1] G. Aad, T. Abajyan, B. Abbott, J. Abdallah, S. Abdel Khalek, A. Abdelalim et al., *Observation of a new particle in the search for the Standard Model Higgs boson with the ATLAS detector at the LHC*, *Physics Letters B* **716** (2012) 1 [[1207.7214](#)].
- [2] S. Chatrchyan, V. Khachatryan, A. Sirunyan, A. Tumasyan, W. Adam, E. Aguilo et al., *Observation of a new boson at a mass of 125 GeV with the CMS experiment at the LHC*, *Physics Letters B* **716** (2012) 30 [[1207.7235](#)].
- [3] O. S. Brüning, P. Collier, P. Lebrun, S. Myers, R. Ostojic, J. Poole et al., *LHC Design Report*, CERN Yellow Reports: Monographs. CERN, Geneva, 2004, [10.5170/CERN-2004-003-V-1](#).
- [4] M. Benedikt, A. Blondel, O. Brunner, M. Capeans Garrido, F. Cerutti, J. Gutleber et al., *FCC-ee: The Lepton Collider: Future Circular Collider Conceptual Design Report Volume 2. Future Circular Collider*, tech. rep., CERN, Geneva, Dec, 2018. [10.1140/epjst/e2019-900045-4](#).
- [5] C. Adolphsen, M. Barone, B. Barish, K. Buesser, P. Burrows, J. Carwardine et al., *The International Linear Collider Technical Design Report*, tech. rep., ILC, Geneva, Jun, 2013.
- [6] The CEPC Study Group, *CEPC Conceptual Design Report: Volume 2 - Physics & Detector*, [1811.10545](#).
- [7] L. Linssen, A. Miyamoto, M. Stanitzki and H. Weerts, *Physics and Detectors at CLIC: CLIC Conceptual Design Report*, [1202.5940](#).
- [8] T. E. S. Group, *Deliberation document on the 2020 Update of the European Strategy for Particle Physics*, tech. rep., ECFA, Geneva, 2020. [10.17181/ESU2020Deliberation](#).
- [9] J. de Blas, M. Cepeda, J. D’Hondt, R. Ellis, C. Grojean, B. Heinemann et al., *Higgs Boson studies at future particle colliders*, *Journal of High Energy Physics* **2020** (2020) [[1905.03764](#)].
- [10] D. d’Enterria, *Higgs physics at the Future Circular Collider*, [1701.02663](#).
- [11] P. Azzi, L. Gouskos, M. Selvaggi and F. Simon, *Higgs and top physics reconstruction challenges and opportunities at FCC-ee*, *The European Physical Journal Plus* **137** (2021) [[2107.05003](#)].
- [12] F. An, Y. Bai, C. Chen, X. Chen, Z. Chen, J. G. da Costa et al., *Precision higgs physics at the CEPC*, *Chinese Physics C* **43** (2019) 043002 [[1810.09037](#)].
- [13] D. M. Asner, T. Barklow, C. Calancha, K. Fujii, N. Graf, H. E. Haber et al., *ILC Higgs White Paper*, [1310.0763](#).
- [14] A. Albert, M. J. Basso, S. K. Bright-Thonney, V. M. M. Cairo, C. Damerell, D. Egana-Ugrinovic et al., *Strange quark as a probe for new physics in the higgs sector*, [2203.07535](#).
- [15] H. Abramowicz, A. Abusleme, K. Afanaciev, N. A. Tehrani, C. Balázs, Y. Benhammou et al., *Higgs physics at the CLIC electron–positron linear collider*, *The European Physical Journal C* **77** (2017) [[1608.07538](#)].
- [16] DELPHI Collaboration, *b-tagging in DELPHI at LEP*, *The European Physical Journal C* **32** (2004) 185 [[hep-ex/0311003](#)].

- [17] J. Prorior, A. Falvard, P. Henrard, J. Jousset and B. B., *Tagging B quark events in ALEPH with neural networks: comparison of different methods*, *Int. J. Neural Syst.* **3 Supp.** (1991) 267.
- [18] V. Abazov, B. Abbott, M. Abolins, B. Acharya, M. Adams, T. Adams et al., *b-jet identification in the D0 experiment*, *Nuclear Instruments and Methods in Physics Research Section A: Accelerators, Spectrometers, Detectors and Associated Equipment* **620** (2010) 490 [[1002.4224](#)].
- [19] J. Freeman, T. Junk, M. Kirby, Y. Oksuzian, T. Phillips, F. Snider et al., *Introduction to HOBIT, a b-jet identification tagger at the CDF experiment optimized for light higgs boson searches*, *Nuclear Instruments and Methods in Physics Research Section A: Accelerators, Spectrometers, Detectors and Associated Equipment* **697** (2013) 64 [[1205.1812](#)].
- [20] ATLAS Collaboration, *ATLAS flavour-tagging algorithms for the LHC Run 2 pp collision dataset*, 2022. [10.48550/ARXIV.2211.16345](#).
- [21] CMS collaboration, *Identification of heavy-flavour jets with the CMS detector in pp collisions at 13 TeV*, *JINST* **13** (2018) P05011 [[1712.07158](#)].
- [22] H. Qu and L. Gouskos, *ParticleNet: Jet Tagging via Particle Clouds*, *Phys. Rev. D* **101** (2020) 056019 [[1902.08570](#)].
- [23] E. Bols, J. Kieseler, M. Verzetti, M. Stoye and A. Stakia, *Jet flavour classification using DeepJet*, *Journal of Instrumentation* **15** (2020) P12012 [[2008.10519](#)].
- [24] J. Erdmann, *A tagger for strange jets based on tracking information using long short-term memory*, *Journal of Instrumentation* **15** (2020) P01021.
- [25] Y. Nakai, D. Shih and S. Thomas, *Strange Jet Tagging*, [2003.09517](#).
- [26] J. Erdmann, O. Nackenhorst and S. V. Zeißner, *Maximum performance of strange-jet tagging at hadron colliders*, *JINST* **16** (2021) P08039 [[2011.10736](#)].
- [27] H. Luo, M.-x. Luo, K. Wang, T. Xu and G. Zhu, *Quark jet versus gluon jet: fully-connected neural networks with high-level features*, *Sci. China Phys. Mech. Astron.* **62** (2019) 991011 [[1712.03634](#)].
- [28] D. Guest, J. Collado, P. Baldi, S.-C. Hsu, G. Urban and D. Whiteson, *Jet Flavor Classification in High-Energy Physics with Deep Neural Networks*, *Phys. Rev. D* **94** (2016) 112002 [[1607.08633](#)].
- [29] P. T. Komiske, E. M. Metodiev and M. D. Schwartz, *Deep learning in color: towards automated quark/gluon jet discrimination*, *JHEP* **01** (2017) 110 [[1612.01551](#)].
- [30] ATLAS collaboration, *Quark versus Gluon Jet Tagging Using Jet Images with the ATLAS Detector*, .
- [31] V. Mikuni and F. Canelli, *ABCNet: An attention-based method for particle tagging*, *Eur. Phys. J. Plus* **135** (2020) 463 [[2001.05311](#)].
- [32] H. Qu, C. Li and S. Qian, *Particle Transformer for Jet Tagging*, [2202.03772](#).
- [33] A. Vaswani, N. Shazeer, N. Parmar, J. Uszkoreit, L. Jones, A. N. Gomez et al., *Attention Is All You Need*, [1706.03762](#).
- [34] F. Bedeschi, *A detector concept proposal for a circular e+e- collider*, *PoS ICHEP2020* (2021) 819.



- [35] FCC collaboration, *FCC Physics Opportunities: Future Circular Collider Conceptual Design Report Volume 1*, *Eur. Phys. J. C* **79** (2019) 474.
- [36] B. Auchmann, W. Bartmann, M. Benedikt, J.-P. Burnet, P. Craievich, M. Giovannozzi et al., *FCC Midterm Report*, *CDS* (2024) .
- [37] N. Bacchetta, J. J. Blaising, E. Brondolin, M. Dam, D. Dannheim, K. Elsener et al., *CLD – A Detector Concept for the FCC-ee*, [1911.12230](#).
- [38] B. Francois, *Noble liquid calorimetry for a future FCC-ee experiment*, *Nuclear Instruments and Methods in Physics Research Section A: Accelerators, Spectrometers, Detectors and Associated Equipment* **1040** (2022) 167035.
- [39] “FCC-ee IDEA detector Delphes card.”  
[https://github.com/delphes/delphes/blob/master/cards/delphes\\_card\\_IDEA.tcl](https://github.com/delphes/delphes/blob/master/cards/delphes_card_IDEA.tcl).
- [40] J. de Favereau, C. Delaere, P. Demin, A. Giammanco, V. Lemaître, A. Mertens et al., *DELPHES 3: a modular framework for fast simulation of a generic collider experiment*, *Journal of High Energy Physics* **2014** (2014) [[1307.6346](#)].
- [41] C. Bierlich, S. Chakraborty, N. Desai, L. Gellersen, I. Helenius, P. Ilten et al., *A comprehensive guide to the physics and usage of PYTHIA 8.3*, [2203.11601](#).
- [42] M. Cacciari, G. P. Salam and G. Soyez, *FastJet user manual*, *The European Physical Journal C* **72** (2012) [[1111.6097](#)].
- [43] S. Catani, Y. L. Dokshitzer, M. Olsson, G. Turnock and B. R. Webber, *New clustering algorithm for multi - jet cross-sections in  $e^+ e^-$  annihilation*, *Phys. Lett. B* **269** (1991) 432.
- [44] M. Cacciari, G. P. Salam and G. Soyez, *The anti- $k_t$  jet clustering algorithm*, *Journal of High Energy Physics* **2008** (2008) 063–063 [[0802.1189](#)].
- [45] T. Suehara and T. Tanabe, *LCFIPlus: A framework for jet analysis in linear collider studies*, *Nuclear Instruments and Methods in Physics Research Section A: Accelerators, Spectrometers, Detectors and Associated Equipment* **808** (2016) 109 [[1506.08371](#)].
- [46] K. Gautam, *Flavour Identification Techniques*, tech. rep., University of Copenhagen, 2020.
- [47] “FCC Physics Analyses using RDataFrame.” <https://github.com/HEP-FCC/FCCAnalyses>.
- [48] F. Bedeschi, “Vertex Fitter in FCCAnalyses.” <https://github.com/HEP-FCC/FCCAnalyses/blob/master/analyzers/dataframe/src/VertexFitterSimple.cc>.
- [49] J. Devlin, M.-W. Chang, K. Lee and K. Toutanova, *Bert: Pre-training of deep bidirectional transformers for language understanding*, 2019.
- [50] D. Buskulic, D. Casper, I. De Bonis, D. Decamp, P. Ghez, C. Goy et al., *Performance of the ALEPH detector at LEP*, *Nuclear Instruments and Methods in Physics Research Section A: Accelerators, Spectrometers, Detectors and Associated Equipment* **360** (1995) 481.
- [51] CMS collaboration, *Particle-Flow Event Reconstruction in CMS and Performance for Jets, Taus, and MET*, tech. rep., CERN, Geneva, 4, 2009.
- [52] A. J. Larkoski, J. Thaler and W. J. Waalewijn, *Gaining (Mutual) Information about Quark/Gluon Discrimination*, *JHEP* **11** (2014) 129 [[1408.3122](#)].
- [53] PARTICLE DATA GROUP collaboration, *Review of Particle Physics*, *PTEP* **2022** (2022) [083C01](#).

- [54] C. Lippmann, *Particle identification*, *Nuclear Instruments and Methods in Physics Research Section A: Accelerators, Spectrometers, Detectors and Associated Equipment* **666** (2012) 148 [[1101.3276](#)].
- [55] G. Cataldi, F. Grancagnolo and S. Spagnolo, *Cluster counting in helium based gas mixtures*, *Nucl. Instrum. Meth. A* **386** (1997) 458.
- [56] W. Klempt, *Review of particle identification by time-of-flight techniques*, *Nucl. Instrum. Meth. A* **433** (1999) 542.
- [57] E. Nakano, *Belle pid*, *Nuclear Instruments and Methods in Physics Research Section A: Accelerators, Spectrometers, Detectors and Associated Equipment* **494** (2002) 402.
- [58] A. Dosovitskiy, L. Beyer, A. Kolesnikov, D. Weissenborn, X. Zhai, T. Unterthiner et al., *An image is worth 16x16 words: Transformers for image recognition at scale*, 2021.
- [59] K. Fukushima, *Visual feature extraction by a multilayered network of analog threshold elements*, *IEEE Transactions on Systems Science and Cybernetics* **5** (1969) 322.
- [60] A. Paszke, S. Gross, F. Massa, A. Lerer, J. Bradbury, G. Chanan et al., *Pytorch: An imperative style, high-performance deep learning library*, 2019.
- [61] M. R. Zhang, J. Lucas, G. Hinton and J. Ba, *Lookahead optimizer: k steps forward, 1 step back*, [1907.08610](#).
- [62] L. Liu, H. Jiang, P. He, W. Chen, X. Liu, J. Gao et al., *On the variance of the adaptive learning rate and beyond*, [1908.03265](#).
- [63] F. Bedeschi, L. Gouskos and M. Selvaggi, *Jet flavour tagging for future colliders with fast simulation*, *The European Physical Journal C* **82** (2022) .
- [64] K. Gautam, *Jet-Flavour Tagging at FCC-ee*, *PoS ICHEP2022* (2022) 1147 [[2210.10322](#)].
- [65] C. Caputo, G. Chiarello, A. Corvaglia, F. Cuna, B. D’Anzi, N. De Filippis et al., *Particle identification with the cluster counting technique for the idea drift chamber*, *Nuclear Instruments and Methods in Physics Research Section A: Accelerators, Spectrometers, Detectors and Associated Equipment* **1048** (2023) 167969 [[2211.04220](#)].
- [66] N. Bacchetta, J. J. Blaising, E. Brondolin, M. Dam, D. Dannheim, K. Elsener et al., *CLD – A Detector Concept for the FCC-ee*, [1911.12230](#).
- [67] L. Breiman, *Random forests*, *Machine Learning* **45** (2001) 5.
- [68] A. Fisher, C. Rudin and F. Dominici, *All models are wrong, but many are useful: Learning a variable’s importance by studying an entire class of prediction models simultaneously*, *Journal of Machine Learning Research* **20** (2019) 1.
- [69] M. Cacciari and G. P. Salam, *Pileup subtraction using jet areas*, *Physics Letters B* **659** (2008) 119.
- [70] UA1 collaboration, *Experimental Observation of Lepton Pairs of Invariant Mass Around 95 GeV/c<sup>2</sup> at the CERN SPS Collider*, *Phys. Lett. B* **126** (1983) 398.
- [71] UA2 collaboration, *Evidence for  $Z^0 \rightarrow e^+e^-$  at the CERN  $\bar{p}p$  Collider*, *Phys. Lett. B* **129** (1983) 130.
- [72] M. Woods, *Review of weak mixing angle results at SLC and LEP*, in *International Europhysics Conference on High-energy Physics (HEP 95)*, pp. 31–34, 10, 1995.

- [73] M. Dam, *Tests of the electroweak theory with the DELPHI detector at LEP*, tech. rep., Oslo Univ., 1995.
- [74] ALEPH collaboration, *Measurement of the Z Resonance Parameters at LEP*, *Eur. Phys. J. C* **14** (2000) 1.
- [75] DELPHI collaboration, *Measurement of the Mass and Width of the  $Z^0$  Particle from Multi - Hadronic Final States Produced in  $e^+e^-$  Annihilations*, *Phys. Lett. B* **231** (1989) 539.
- [76] OPAL collaboration, *Measurement of the  $Z^0$  Mass and Width with the OPAL Detector at LEP*, *Phys. Lett. B* **231** (1989) 530.
- [77] MARKII collaboration, *Initial Measurements of Z-boson Resonance Parameters in  $e^+e^-$  Annihilation*, *Phys. Rev. Lett.* **63** (1989) 724.
- [78] ALEPH, DELPHI, L3, OPAL, SLD Collaborations, *Precision Electroweak Measurements on the Z Resonance*, *Physics Reports* **427** (2006) 257 [[hep-ex/0509008](#)].
- [79] SLD collaboration, *First Direct Measurement of the Parity-Violating Coupling of the  $Z^0$  to the s Quark*, *Phys. Rev. Lett.* **85** (2000) 5059.
- [80] SLD collaboration, *SLD Design Report*, tech. rep., SLAC, 5, 1984.
- [81] DELPHI Collaboration, *Letter of Intent: DELPHI detector (DEtector with Lepton Photon + Hadron Identification)*, tech. rep., CERN, Geneva, 1982.
- [82] OPAL Collaboration, *Letter of Intent: "OPAL Detector"*, tech. rep., CERN, Geneva, 1982.
- [83] G. F. von Dardel, A. H. Walenta, E. Lorenz and P. Duinker, *L3: Letter of intent; 1982 ed.*, tech. rep., CERN, Geneva, 1982.
- [84] ALEPH Collaboration, *Letter of Intent: ALEPH detector - Apparatus for LEP PHysics*, tech. rep., CERN, Geneva, 1981.
- [85] DELPHI collaboration, *Measurement of the strange quark forward- backward asymmetry around the  $Z^0$  peak*, .
- [86] Glen Cowan, Eilam Gross, "Discovery significance with statistical uncertainty in the background estimate."  
<https://www.pp.rhul.ac.uk/~cowan/stat/notes/SigCalcNote.pdf>, 2008.
- [87] L. Freitag, *Benefits of Minimizing the Vertex Detector Material Budget at the FCC-ee*, tech. rep., Zurich U., 2023.